TITLE:

Recurrence of the Large Earthquakes associated with the Fukui Earthquake Fault, as Derived from Subsurface Structure, Topography and the Present Day Seismic Activity

AUTHOR(S):

TAKEUCHI, Fumiaki

CITATION:

TAKEUCHI, Fumiaki. Recurrence of the Large Earthquakes associated with the Fukui Earthquake Fault, as Derived from Subsurface Structure, Topography and the Present Day Seismic Activity. Bulletin of the Disaster Prevention Research Institute 1989, 39(4): 91-127

ISSUE DATE:

1989-12

URL:

http://hdl.handle.net/2433/124963

RIGHT:

京都大学学術情報リポジトリ
KURENAI 紅
Kyoto University Research Information Repository

Recurrence of the Large Earthquakes associated with the Fukui Earthquake Fault, as Derived from Subsurface Structure, Topography and the Present Day Seismic Activity

By Fumiaki TAKEUCHI

(Manuscript received September 4th, 1989)

Abstract

Very little has been known about the Fukui earthquake fault, in spite of the fact that it generated one of the largest inland earthquakes in Japan, the 1948 Fukui earthquake (M=7.1). Thus its recurrence characteristics have also been unknown. One main reason for this lack of knowledge of the fault is that its epicentral area is covered by thick deposits.

We carried out a number of geophysical explorations, such as gravity, geomagnetic total force and microtremor measurements, to estimate the location and the vertical offset of the Fukui earthquake fault. The fault is located with a vertical offset of about 200 m, beneath the fissure zone that were caused by the 1948 earthquake.

Because the vertical displacement associated with the 1948 event was roughly 1 m, we concluded that earthquakes of a similar size to the 1948 event have recurred 200 times on the same fault. The average recurrence time was estimated to be about 2,500 years, accepting that the crustal movements in Southwest Japan have been almost constant since the middle Quaternary.

Differences of levels across the fault are evidenced in the surface topography. The local variation of these differences is explicable from the average recurrence time.

An aseismic region was found adjacent to the fault in the aftershock area of 1948 event. This region coincides with that of the region of large surface differences.

Thus, the recurring earthquakes, at least the recent ones, seem to have a similar distribution of vertical dislocation along the fault to that of the 1948 event.

1. Introduction

In Southwest Japan, a number of destructive earthquakes have taken place along the inner side of the arc, as well as the major inter-plate earthquakes located on the Pacific Ocean side (**Fig. 1**). Although the inland destructive earthquakes are usually smaller than the large inter-plate earthquakes, they often cause loss of human lives, destruction of the natural environment and man-made structures. One of such large disastrous earthquakes was the Fukui earthquake of June 28, 1948, which occurred in Fukui prefecture situated in the northeastern part of Southwest Japan. The magnitude was 7.1; 3,895 lives were lost and 35,420 houses totally collapsed (Tsuya, 1950)[2], as the epicenter was located near the highly populated city of Fukui. As an aggravating factor, the thick alluvial deposits that covered the epicentral area played

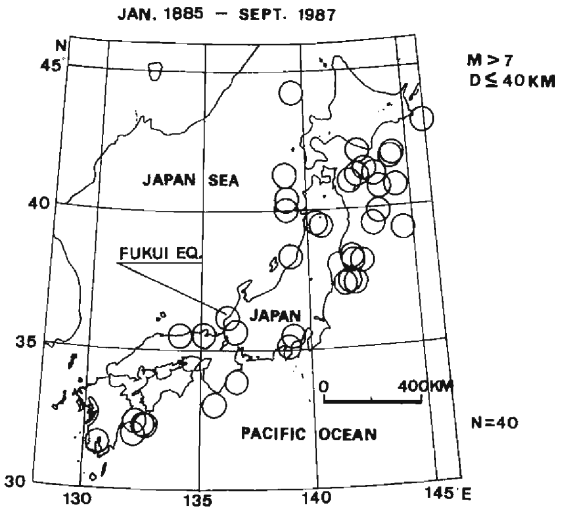

Fig. 1. Distribution of $M>7$ shallow earthquakes in and around Japan from 1885 to 1987. SEIS-PC program (Ishikawa et al., 1985)[1] is used to draw the figure.

a significant role in amplifying ground motion.

This was the first event with magnitudes greater than 7 to occur at this place. No previous events could be traced even in historical documents. Since the study area is located only 100 km away from Kyoto, the old Japanese capital, historical documents on earthquakes of the area are likely to be reliable back to about 1,000 years. No geological evidence for estimating recurrence characteristics of earthquakes has been available, because the thick deposits conceal any such evidence. In fact, though many kinds of surveys were carried out in the epicentral region immediately after the earthquake (Tsuya, 1950)[2], no fault could be detected on the ground surface. Numerous cracks and fissures appearing along a belt trending almost N15°W only could be delineated. Only leveling surveys pointed out that appreciable differences in ground level were created by the earthquake across the fissures (**Fig. 2B**).

A fault plane solution derived from P-wave first motions (Hirono, 1949)[3] showed a left-lateral strike slip mechanism, with one of the nodal planes trending N10°W (**Fig. 2C**), which agreed well with the leveling result. There was also a thrust component, because the leveling survey showed upheaval to the eastern side to the fault and subsidence to the west, with a maximum difference of around 1 m.

Dynamic and static parameters for the fault movement were presented by Kanamori (1973)[4] using the seismic waveforms obtained at the Abuyama Seismological Observatory (epicentral distance, 155 km), Kyoto University, as well as the crustal movement data. He concluded the length of the fault to be 30 km, the width 10 km, the depth to the top of the fault 1 km, horizontal displacement 2 m and vertical displacement 1 m. The seismic moment and the stress drops were derived as 3.3×10^{26} dyne cm and 83 bars, respectively. The fault plane was considered to be almost vertical; however, the fault may be steeply dipping to the east, since most

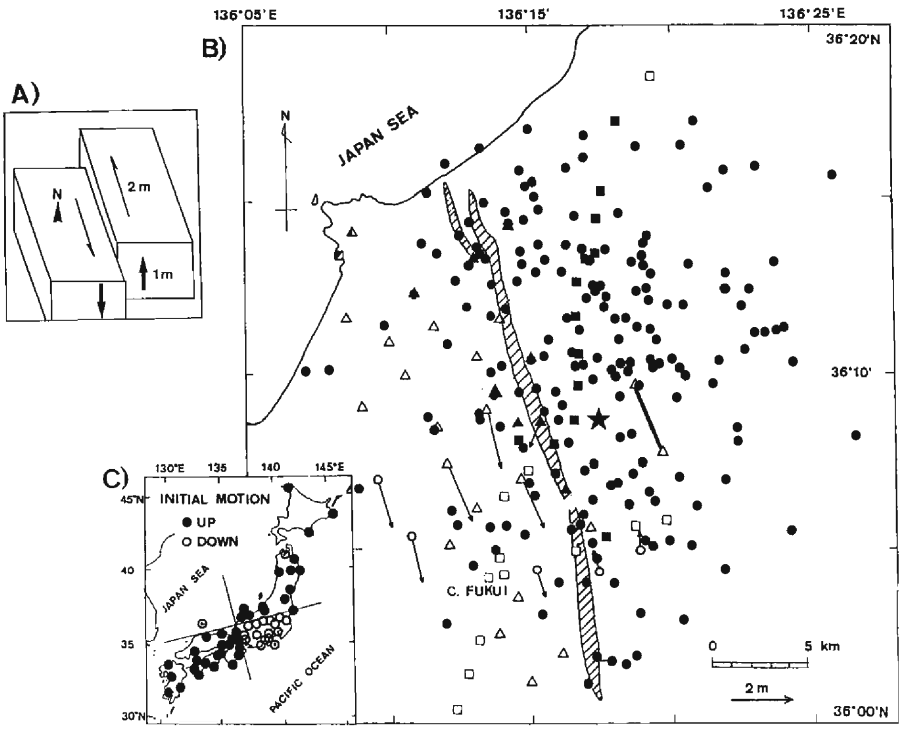

Fig. 2. **A**) Schematic diagram showing the fault movement of the 1948 Fukui earthquake (left-lateral strike slip with easterly upheaval).
B) Aftershock distibution (solid circle) of the Fukui earthquake and results of triangular and leveling surveys. Triangles denote triangular stations, squares are leveling stations (after Tusya, 1950)[2]. Solid squares and triangles represent upheaval and open ones subsidence. Arrows indicate direction of horizontal movement and their length are proportional to the displacement. Hatched areas are the fault zone suggested by fissure distribution which appeared after the earthquake. Star in the center of the figure is the main shock.
C) Up-down distribution of P-wave initial motions (after Hirono, 1949)[3].

aftershocks are distributed along the eastern side of the fault, as is shown in **Fig. 2B**. Kanamori (1973)[4] also showed that the main event consisted of at least two large shocks, with an interval of about 9 seconds between the two. He ascribed the same mechanism to both shocks. However the later shock had a displacement 4 times larger than the former one. More detailed parameters were determined by Hasegawa (1986)[5], who applied a non-linear inversion technique for the crustal movement data and obtained a model of the fault composed of 8 sub-faults. The total length of those faults was determined to be 23 km, shorter than Kanamori's estimation; however, their conclusions concerning location and strike direction were not so much different.

Large inland earthquakes in Japan are thought to occur repeatedly on the same faults or on the same segments of faults (Matsuda, 1975)[6]. Their recurrence times can be directly known, provided the times of occurrence of more than two successive

earthquakes on the same fault are known. Trenching surveys have also revealed such recurrence times in inland Japan (e.g. Ando et al., 1980[7], Okada et al., 1981[8], Disaster Prevention Research Institute, Kyoto University, 1983a[9], 1983b[10]). Another way to calculate the recurrence time is to divide the dislocation associated with one earthquake by the long term slip rate (Wallace, 1970)[11], which rate is estimated from geological or topographical evidence.

Since the Fukui earthquake fault, however, is buried beneath a thick deposit, no geological information can be obtained. The trenching method is not applicable in this region because the location of the fault can be deciphered only very roughly (within about 1 km).

Our main objectives are to establish that a series of earthquakes similar to the Fukui earthquake have occurred repeatedly along the same fault, and to find common characteristics for the past earthquakes as far as possible.

We shall first reveal the existence of a buried fault beneath the thick deposit by carrying out geophysical explorations. Next, the vertical offset across the fault in the sub-surface layers will be estimated; this will lead to an estimation of the average recurrence time of the large earthquakes associated with the fault, because the offset reflects the net vertical displacement caused by the repeated events. In deriving this subsurface structure, we shall make full use of data from our geophysical explorations and shall attempt to produce a reliable model.

In addition, the differences in ground level across the fault will be discussed with reference to the aseismic region which is clearly shown by recent microseismic activity. Through this, some concluding remarks about the similarity of the distribution of dislocation associated with the repeated earthquakes will be made.

2. Tectonic settings

Preceding the 1948 Fukui earthquake, the Nobi earthquake (M=8.0), another large inland earthquake occurred in 1891 adjacent to the southern side of the Fukui region. The 1948 Fukui earthquake could even be one of its large aftershocks, because the Fukui earthquake fault is located at the northern extension of the Neodani fault, the movement of which caused the Nobi earthquake. Again, the Daishoji-Oki earthquake (M=6.9) of 1952, which occurred at the northern edge of the aftershock area of the 1948 Fukui earthquake, might also be one of the aftershocks of the 1948 earthquake. These epicentral regions of three large earthquakes form a 160 km long belt of high seismic activity, as shown in **Fig. 3**.

The epicenter of the 1948 Fukui earthquake is in the Fukui plain, which has a dimension of 10 km in the E-W direction and 20 km in the N-S direction. The average depth to the basement is about 150 m, and the eastern edge of the plain is bounded by mountains of Tertiary volcanic rocks. Cenozoic mountains delineate the southern part of the west boundary of the plain, and the northern part of the plain comes in contact with the Japan Sea. Basement rocks of the plain are also Tertiary (**Fig. 4**). The basement has been subsiding, as a whole, and sedimentation has been

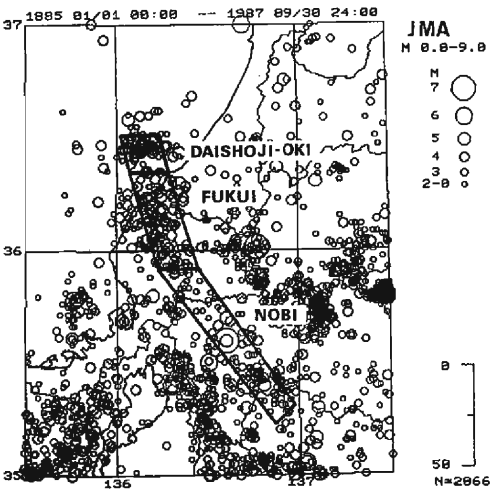

Fig. 3. Seismicity map from 1885 to 1987, showing a belt of aftershock areas of three large inland earthquakes. SEIS-PC program[11] was used to draw the map.

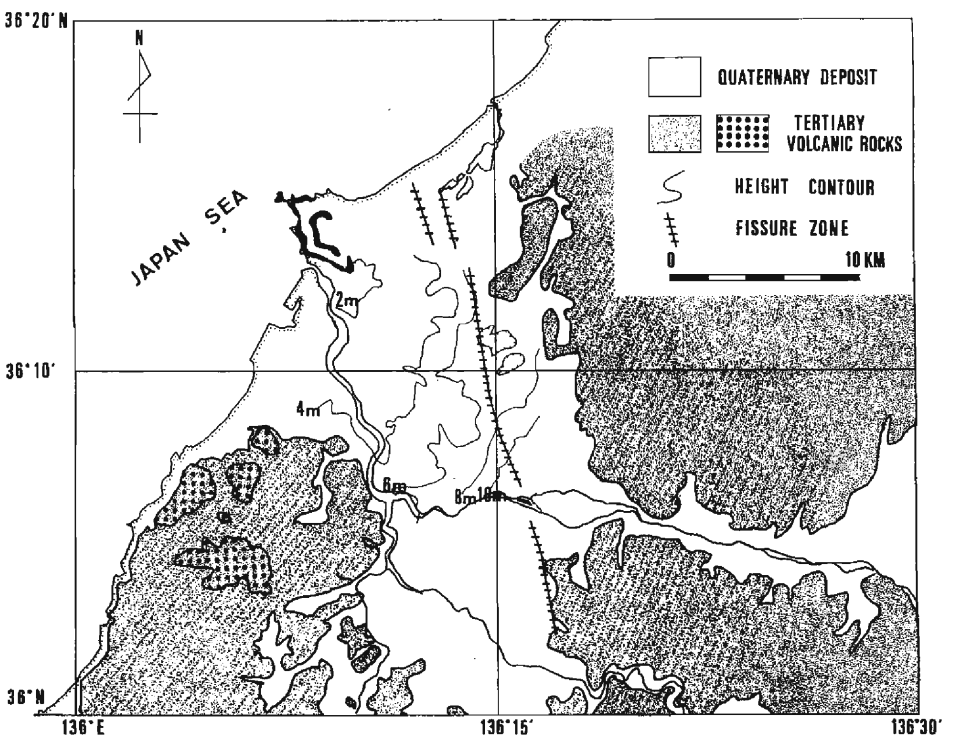

Fig. 4. Simplified Geological map over the area studied with altitude contours in the Fukui plain (modified after Fukui Prefecture, 1969[12] and Hokuriku Nouseikyoku Keikakubu, 1982[13]). The fissure distribution is also shown.

taking place (Hokuriku Nouseikyoku Keikakubu, 1982)[13]. The sediments overlying the basement rocks consist of diluvial and alluvial deposits. The average thickness of the alluvial deposit is around 30 m.

The tectonic strain data at this region has been presented by Geographical Survey Institute (1987)[14]. The data demonstrate that the horizontal compressional strains are oriented between NNW-SSE and WNW-ESE directions in the aftershock area, which agrees with the direction of the P axis for the mainshock of 1948 as suggested by the push-pull distribution cited in **Fig. 2C**[3]. This direction holds also for the P axes of the majority of recent micro- to small-earthquakes (Takeuchi, 1988)[15].

3. Location of the fault and estimation of its vertical offset

The fault plane of the 1948 event is supposed to lie almost vertically beneath the Fukui plain. If earthquakes of this type had occurred repeatedly in the same manner as that of the 1948 event, the fault offsets in both vertical and horizontal directions should have grown with time. Although the horizontal offset ought to have been twice as large as the vertical one, the vertical offset is much easier to detect by geophysical explorations.

Among the many boundaries between layers, the one between the basement rock and the sediment is the one we wish to determine the accurate depth of, because the contrast in elastic coefficients across this boundary is normally the largest. Moreover, deeper structures than this are more difficult to determine precisely, while the shallower deposits would also not fully reflect the accumulation of the vertical dislocations by the repeated earthquakes, because some of the upper layers could have been lost by erosion.

The offset in the basement rocks can be expressed simply by D multiplied by M, where D is the vertical displacement caused by each earthquake and M the total number of such earthquakes. This method is applicable to the region concerned, where the basement structure was formed in the middle Pleistocene (Hokuriku Nouseikyoku Keikakubu, 1982)[13], and since then the basement rocks have been subsiding as a whole (Kaseno et al., 1972)[16]. Thus the net vertical offset of the basement rocks, which has been formed by repeated earthqukaes is, likely to be preserved without being eroded.

3.1 Data suggesting the fault location and the offset, before our surveys

A rough location of the fault was suggested from microearthquake distribution (Takeuchi and Hirano, 1985)[17]. **Figure 5** shows the seismic activity obtained by the Hokuriku Microearthquake Observatory, Disaster Prevention Research Institute, Kyoto University, from May 1976 to Dec. 1984. The aftershock distribution of the 1948 Fukui earthquake, forming a clear belt, can be easily recognized. The fault length could be estimated as 30 km, with a strike of roughly N15°W, thus agreeing well with the fault model of Kanamori (1973)[4]. However, the distribution is not along a sharp line, but shows a spread of about 10 km in width. Distribution of the

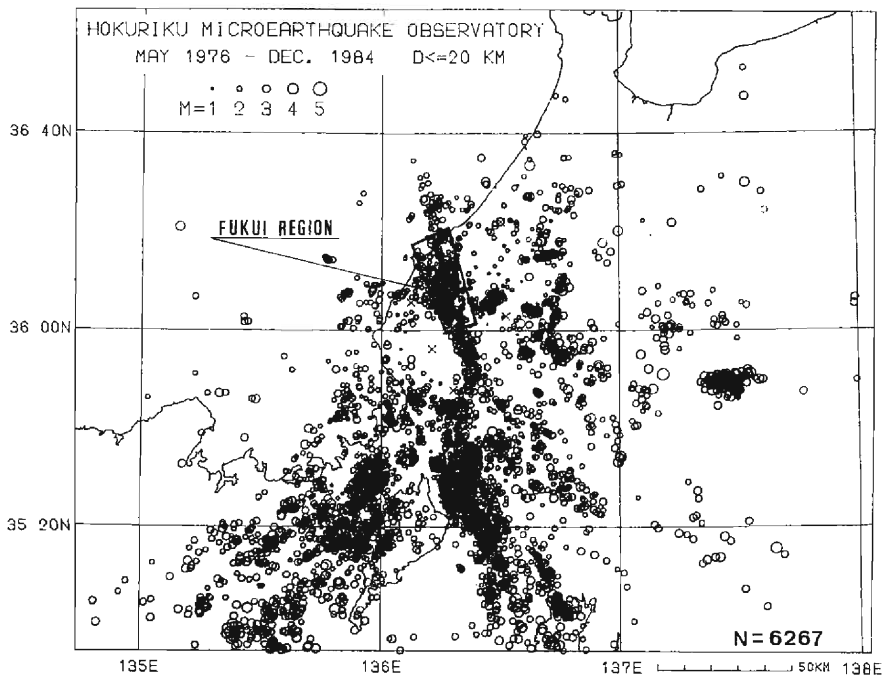

Fig. 5. Microearthquake distribution presented by the Hokuriku Microearthquake Observatory, Kyoto University from May 1976 through Dec. 1984 (after Takeuchi and Hirano, 1985)[17]. The aftershock distribution of the 1948 Fukui earthquake form a belt with a width of about 10 km.

aftershocks just following the main shock (**Fig. 2B**) also exhibits an even wider spread. Thus, the seismicity suggests only a very rough possible range for the location of the fault.

As for the offset, we shall present two comparative illustrations. One is a band-passed (passed wave-length: 8–20 km) contour map of the Bouguer anomalies in and around the epicentral area (**Fig. 6A**)[18]. The other is a contour map of the ground displacements caused by the 1948 earthquake (**Fig. 6B**), for which the leveling data (Tsuya, 1950)[2] were used. The two patterns resemble each other very well in the sense that the high values are distributed to the east of the fissure alignment and the low values to the west. The locations of two lows and a high are also quite conforming. The difference between the highest and the lowest values of the Bouguer anomalies amounts to about 5 mgals, which value is of two orders larger than the change of the Bouguer anomaly caused by the 1948 earthquake. This shows that the accumulated vertical offset is large enough to detect by geophysical explorations.

3.2 Gravity and Geomagnetic Surveys

We carried out gravity and geomagnetic surveys to determine accurately the location and the offset of the fault. **Figure 7A** shows the area studied. The fissure

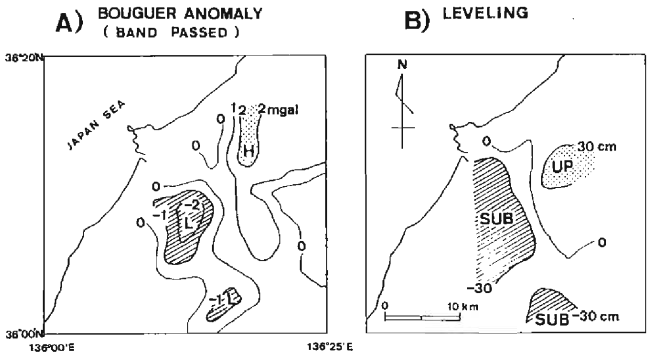

Fig. 6. Resemblance between **A**) the present Bouguer anomaly (after Suzuki, 1982)[18], for which a band-pass filter (passed wave-length; 8–20 km) is applied and *B*) the result of leveling surveys (modified after Tsuya, 1950)[2]. The Bouguer anomaly is about 2 orders greater than that expected by the displacements associated with the 1948 event.

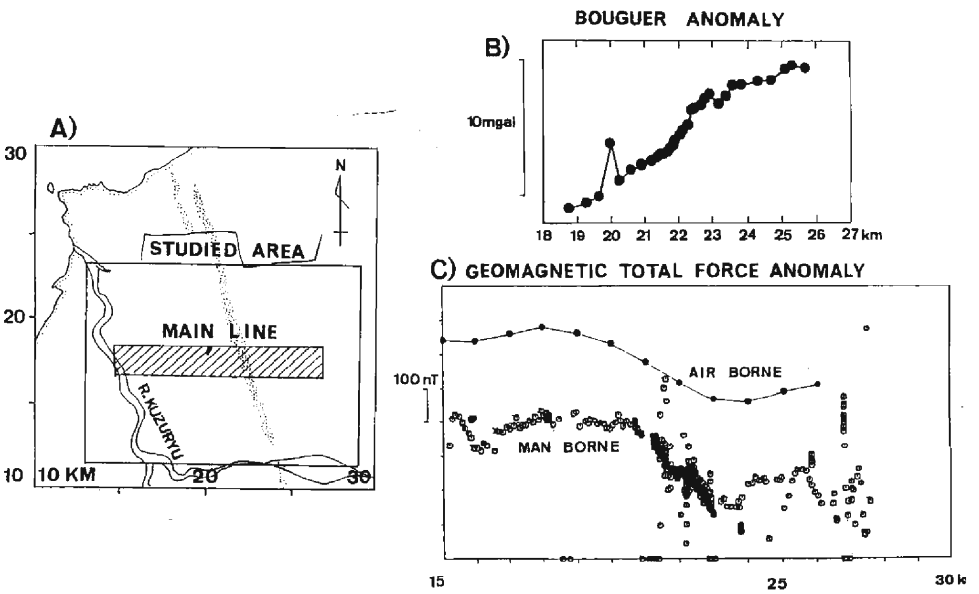

Fig. 7. **A**) Map showing the area studied. Hatched area is referred to as the main line. Shaded belts are the fissure zones.
B) Observed Bouguer anomalies along the main line.
C) Anomaly of geomagnetic total force along the main line (open circles), for which time variation is corrected. Solid circles indicate observed data at a height of 1,500 ft. above the ground obtained by Geological Survey of Japan (1975)[22].

zone that appeared after the main shock is shaded. A number of explorations were carried out in the hatched rectangle region. This region will be referred to as the main line throughout this article. Numerals in the vertical and horizontal axes show

the distances in km in two perpendicular directions, as measured from a reference point (36°N, 136°E). Eastwards and northwards should be considered as the x and y directions, respectively.

(1) Gravity survey along the main line

Gravity measurements were made by two LaCoste & Romberg gravimeters. The number of grid points along the main line was 40, with an average spacing of 200 m. The Bouguer and the terrain corrections were applied assuming 2.67 g/cm^3 as the average density. For more detailed procedure, one should refer to our earlier paper (Takeuchi et al., 1983)[19]. A number of observation points were located on bench marks, where the altitudes were known within an accuracy of 1 mm (as determined by the Geographical Survey Institute). For the remaining points, large scale topographical maps issued by towns, villages and the city in the study area were used. The accuracy of the altitudes presented in these maps has been discussed in another paper (Takeuchi and Amaike, 1985)[20], and was found to be around 10 cm in the observed area of flat rice fields. This would generate an error of only 0.02 mgal in the Bouguer anomaly. The residual Bouguer anomalies were plotted in **Fig. 7B**. A regional trend of 0.235 mgal/km towards N76°W (Hibi, 1982)[21] for this district was subtracted from the data.

(2) Geomagnetic survey along the main line

Our observation points were located very densely along the main line, with a spacing of 10 to 100 m. Two portable sets of Barringer magnetometers were employed. The data at an observation point could be easily taken in a couple of minutes. The data quality was much affected by the presence of artificial constructions. As a matter of fact, buildings, railways, electrical wires, cars and even a small iron nail can be noise sources. In order to avoid these disturbances, observation points were mainly located in the central part of the nearly square rice fields, and no building was usually near them. In addition, there were hardly any iron objects in these paddy fields.

The sensors were supported on the top of a 2 m long pole held by the observer. As the studied region is very flat, no terrain correction was needed. Data accuracy was checked during the field survey. A number of data taken at the same point in a few minutes were compared and the deviation was found to be within a few nT, thus testifying to the accuracy. The relative location of the spot where the observer stands with respect to the sensor, also affects the data, however the magnitude of the error is very small and does not exceed 10 nT. Thus, we measured only one value at each point, holding the sensor west of the observer, because such an alignment more or less gave the average value in all directions. When the point could not be taken in the rice field, unpaved roads were used. In this case the deviation was relatively greater, but still negligible.

To eliminate the effect of the time variation of the magnetic field, the base level at the Tottori Microearthquake Observatory of the Disaster Prevention Research

Institute, Kyoto University, located in Tottori prefecture, 200 km SWW of the study area, were subtracted from each observed datum. The corrected data along the main line are plotted in **Fig. 7C**. Data by an airborne observation at a height of 1,500 ft above the ground carried out by the Geological Survey of Japan (1975)[22] are also shown in the same figure by solid circles.

(3) Analysis and Results from Surveys

A subsurface structural model which can explain both the gravity anomalies and the magnetic field along the main line was searched for by the trial and error method. Calculations were based on 2-dimensional models. For gravity, the method proposed by Talwani et al. (1959)[23] was used. For geomagnetic total force anomaly ΔT, the theoretical formalism by Grant et al. (1965)[24] for a ramp structure was employed (see **Fig. 8B** for geometry).

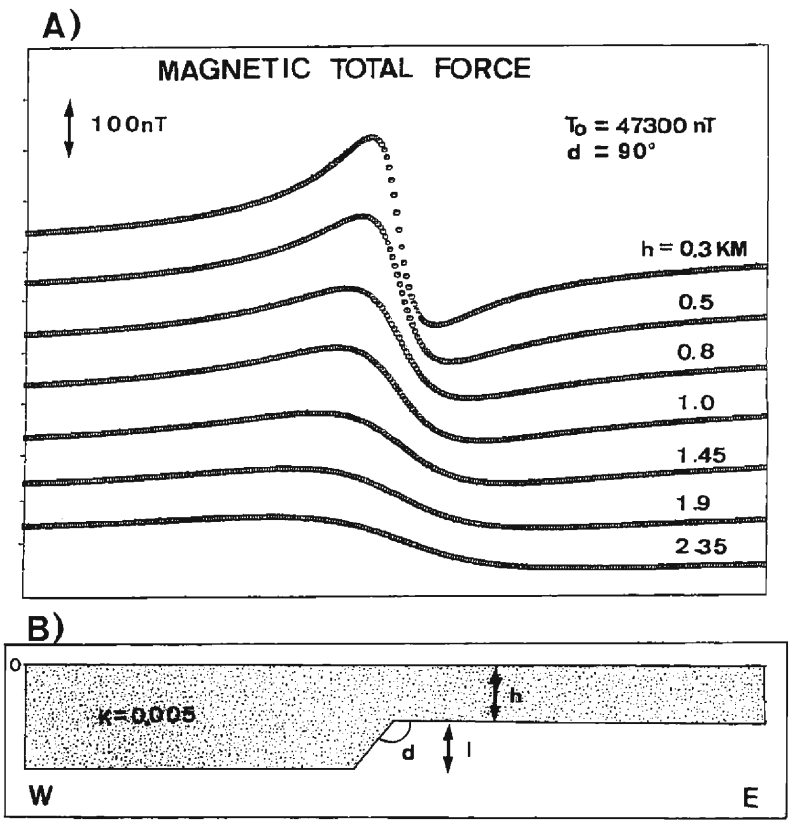

Fig. 8. **A**) Examples of theoretical values of magnetic total force calculated for the subsurface structure shown in figure **B**). The local intensity, T_0 was fixed to be 47,300 nT, and d=90° was also assumed. Curves are drawn for different values of h.

B) Assumed subsurface structure.

$$\Delta T/[2*k*T_0*(1-\cos^2 i*\cos^2\lambda)]$$
$$=\sin d*\cos(d-2\beta)*\ln[\{(x-l*\cot d)^2+(h+l)^2\}/(x^2+h^2)]^{1/2}$$
$$+\sin d*\sin(d-2\beta)*[\tan^{-1}\{(x-l*\cot d)/(h+l)\}-\tan^{-1}(x/h)],$$

where T_0 and i are respectively the local intensity and the declination of the geomagnetic field, λ the strike of the structure, d the dipping angle of the step edge measured clockwise from the right horizon, h and x are respectively the vertical and the horizontal distances from the observer to the top of the step, l the height of the step and k the susceptibility. Symbol * is used for arithmetic multiplication (not convolution) throughout this article. β is an angle defined by the relation,

$$\tan\beta=\tan i/\sin\lambda.$$

A 3-layer model is assumed. The layers are 1) sediments made up of alluvial and diluvial deposits, 2) the basement rocks and 3) the deeper formations. The basement rocks are Tertiary, as revealed by the boring data (Hokuriku Nouseikyoku Keikakubu, 1977)[25], and layer 3) is identified as the granitic layer. Densities for these layers are assumed to be 2.0, 2.4 and 2.6 g/cm^3, respectively. These values were also used for this region by Kono et al. (1981)[26]. In layer 1), the density of the alluvial sediment might be about 1.6 g/cm^3, much smaller than the diluvial sediments; however, this difference can be neglected because the thickness of the alluvial sediment is very small so that the difference originating from this density assumption is negligible.

The lower boundary of the basement in contact with the granitic layer was determined mainly by magnetic survey data. The magnetic total force along the main line are high in the western part, and they decrease to the east, in contrary to the gravity anomaly. The maximum and minimum values appear at distances of 20 km and 23.5 km, respectively, in the x direction, as shown in **Fig. 7C**, if the small fluctuations are smoothed. The difference between the maximum and the minimum values is around 300 nT. This anomaly originates from the deeper structure, i.e., the undulation of the boundary between the granitic layer and the basement rocks.

In the middle part of the graph, a variation in the shape of a rotated S can also be seen. This fluctuation has a shorter wave-length, reflecting the shallower structure, i.e., the boundary between the basement rocks and the overlying sediments. This is the main target in our structural analysis. However, as shown above, as the long wave-length anomalies are superposed on the shorter ones, the deeper structure should be at first derived and its effect on the magnetic field should be subtracted from the observed data.

(a) Long wave-length data

The basement rocks consist of Tertiary volcanic materials, whose susceptibility is higher than that of the underlying layer (Granitic layer). Then the long wave-length anomaly, high in the west and low in the east, suggests a model with an eastward ascending boundary between these two layers. The observed gravity anomalies

show high values in the east and low in the west, contrary to the magnetic anomalies. However, this also supports the above model, because the density of the basement rocks is lower than that of the granitic layer, contrary to the case of susceptibility. So we have modeled for both the gravity and magnetic anomaly data assuming a step-like (or ramp-shape) structure with the eastern side elevated.

Figure 8A illustrates the magnetic total force field calculated from the subsurface structure outlined in **Fig. 8B**. The offset and the dip angle were kept at 1 km and 90°, respectively. The intensity of the field is proportional to the susceptibility difference between the two layers. We have used the susceptibility difference, $k=0.005$, which is reasonable for volcanic rocks. The shape of the magnetic field anomaly depends on h, which is, in turn, governed by two parameters. One is "amplitude", which is the difference between the maximum and the minimum of the total force anomaly, and the other is "width", which is the horizontal distance be-

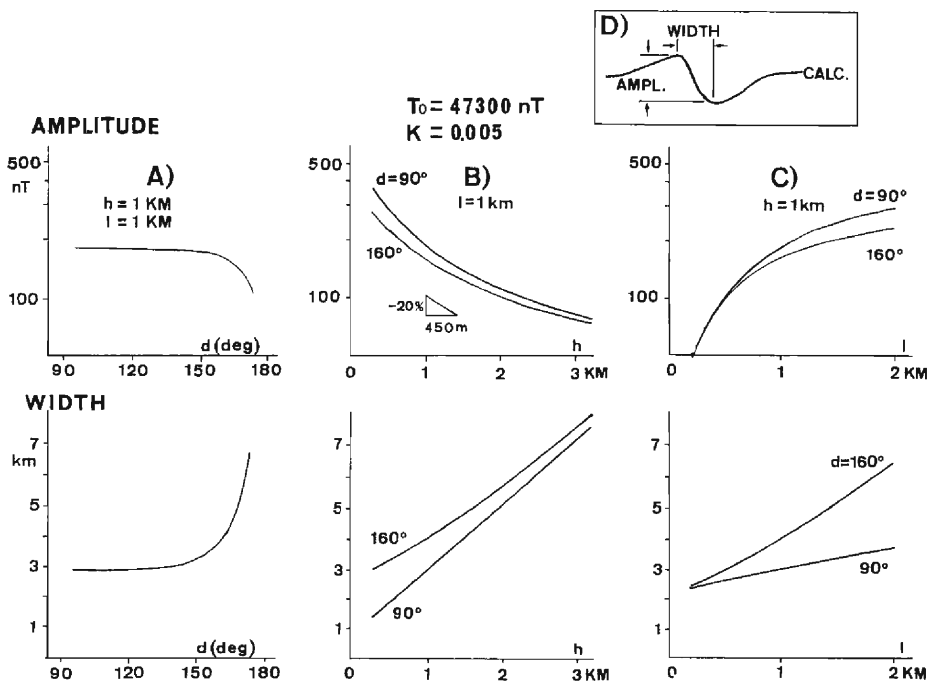

Fig. 9. 'Amplitude' and 'width' versus parameters that represent the subsurface structure. Definition of 'Amplitude' and 'Width' are shown in figure **D**).

A) 'Amplitude' and 'Width' versus the dip angle d. Both h and l are fixed to be 1 km. Between 90° and 160°, d does not much affect either 'Amplitude' or 'Width'.

B) 'Amplitude' and 'Width' versus h for cases of $d=90°$ and 160°. Parameter l is fixed at 1 km. The hypotenuse of the triangle in the upper figure shows a rate of −20% for 'Amplitude' when h increases by 450 m (1,500 ft.). The derivative of the curve for $d=160°$ is parallel to the hypotenuse when $h=1$ km.

C) 'Amplitude' and 'Width' versus l, h is also fixed to be 1 km.

D) Schematic diagram showing the definition of 'Amplitude' and 'Width'.

tween those two points. With constant l and k, as the depth increases, the "amplitude" decreases, and the "width" increases. If the dip angle d remains within the range between 90° and 160°, d does not significantly affect the magnetic field, as shown in **Fig. 9A**.

Figure 9B shows the "amplitude" (upper figure) and "width" (lower figure) versus depth for the two extreme values of $d=90°$ and $d=160°$. The observed "width" is around 3.5 km, which can be simulated by taking $h>0.8$ km ($d=160°$) or $h>1.3$ km ($d=90°$). However, when the air borne data is taken into account, there is an upper limit for h. The "amplitude" for the air borne data taken at an altitude of 1,500 ft. (450 m) above the main line is estimated to be 240 nT, which is 20% less than that for the ground measured data (300 nT).

The hypotenuse of the triangle in **Fig. 9B** shows a rate of 20% decrease of "amplitude" when h increased by 450 m. The value of h, at which the derivative of the theoretical curve is parallel to the hypotenuse of the triangle, is a possible depth to the granitic layer below the ground surface. The depth is 1 km when $d=160°$, and 2 km when $d=90°$.

The offset l also affects these parameters. **Figure 9C** shows the "amplitude" (upper) and the "width" (lower) as functions of l, with $h=1$ km. The "width" well represents the actual data of 3.5 km when l equals to 1 km for the case of $d=160°$ as shown in **Fig. 9C**. However, the "amplitude" is 180 nT, which is only about 60% of the observed amplitude of 300 nT. This shows that the value of k should be increased to 0.008, because the 'amplitude' is proportional to k. As the width is not affected by changing the value for k, the combination of parameters ($h=1$ km, $l=1$ km, $d=160°$) satisfies the observed data. This model will be used as the final one to explain the long wave-length anomaly. However, other combinations of parameters l and d are also permitted. For an example, $l=1.9$ km and $d=90°$ also is a possible case with keeping h to be 1 km. The reason why we chose the above model as the final one is that it required the most gentle slope for the ramp structure, i.e., d is largest, among possible cases.

(b) Short wave-length data

By subtracting the long wave-length anomaly, caused by the model structure as derived in the previous section, from the observed data, we may estimate the boundary structure between the basement rock and overlying sediment. Our main purpose is to obtain the offset of this boundary.

The trial and error method was again employed. The final model was rather easily reached. Since the short wave-length data variation of the geomagnetic anomaly was much smaller than that of the long wave-length component, and hence the model structure could be changed without affecting the long wave-length component during the trial and error process, we could search for an appropriate model regardless of the air borne data. The final subsurface structure model is shown in **Fig. 10C**. The offset of the concerned boundary was determined to be 200 m, as shown by a circle in the figure. Good agreement between observed and calculated

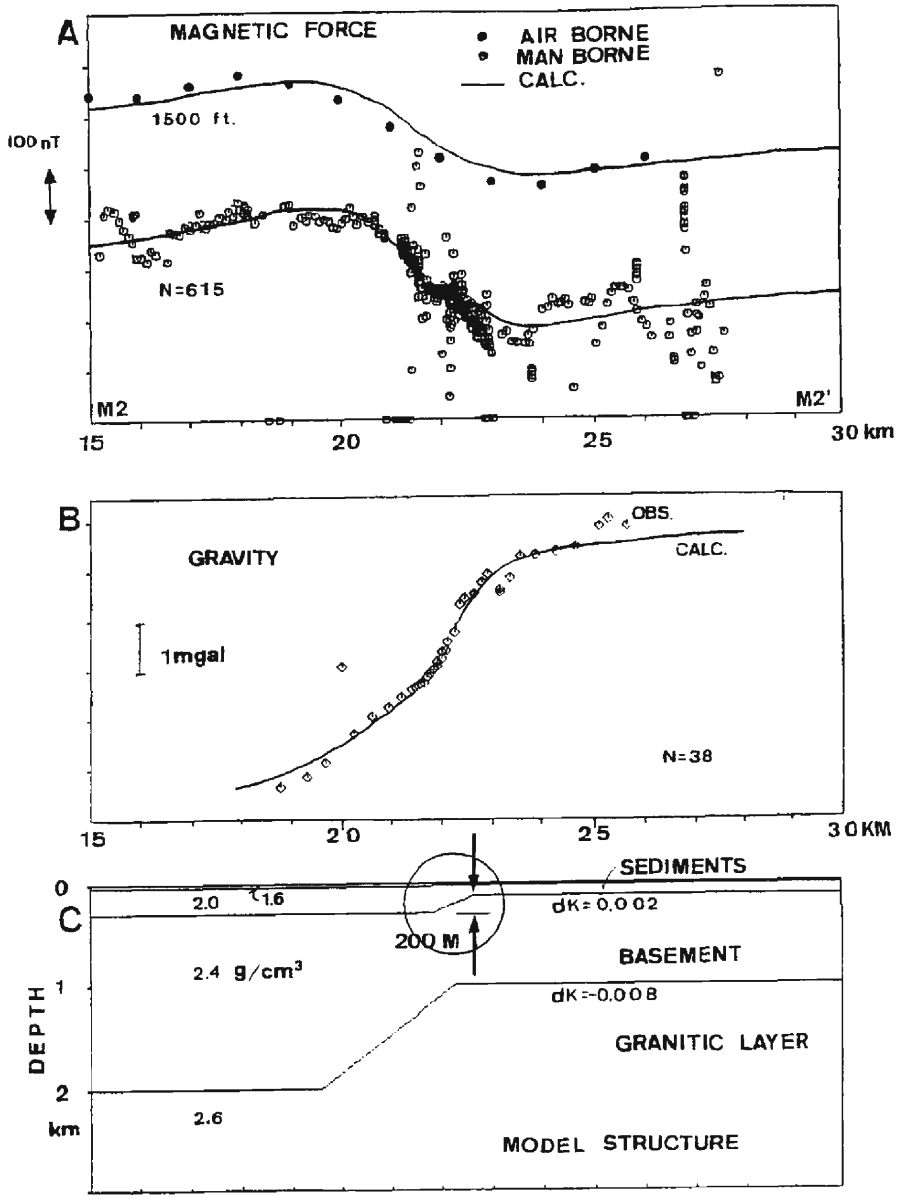

Fig. 10. **A)** Observed (circle) and calculated (solid line) values of magnetic anomaly. Open circles indicate the data obtained at the ground surface, and solid circles denote those data obtained at a height of 1,500 ft. by Geological Survey of Japan[22]. Calculation was based on the subsurface structure shown in the bottom figure. Good agreement is shown between observed and calculated values of long wave-length components. A rotated S shape of the observed data is superposed on the long wave-length component. For agreement with calculated values, See **Fig. 11.**

B) Observed and calculated gravity anomaly. Calculation is based on the

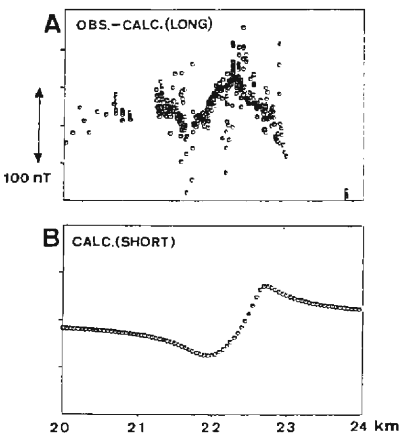

Fig. 11. Short wave-length component of magnetic anomaly.
A) Observed data from which the theoretical values of long wave-length component were subtracted. The trough and peak at the center of the figure correspond to the rotated S shape in **Fig. 10A**.
B) Theoretical anomaly which is calculated from the subsurface structure shown in the circle in **Fig. 10C**.

values of the magnetic field is demonstrated in **Fig. 10A** and that for the gravity fields is shown in **Fig. 10B**. Solid lines in both figures show the calculated values which are derived from the subsurface structure model shown in **Fig. 10C**.

Figure 11A shows the short wave-length component of the observed magnetic data. This is the rotated S variation shown in the range of $x=20$ to 24 km in **Fig. 10A**, from which the theoretical field calculated for the ramp structure as derived above is subtracted. **Figure 11B** is the calculated field based on the stractural model encircled in **Fig. 10C**. Again, the observed and calculated fields agree well with each other, indicating that the derived model well explains the observation.

3.3 Re-examination of the location and offset by Seismic Exploration

The structural model derived in the previous section revealed the location and the vertical offset of the fault. However, their resolutions are not so high, because there exists a trade-off between the offset and the contrast of physical constants. To ascertain the offset in the upper boundary, i.e., the boundary between the sediments and the basement rock, a seismic survey was applied in the central part of the main line.

As the details of the seismic survey has been explained in another paper (Amaike et al., 1984)[27], we describe it only briefly here. The length of our survey line was

structure in the bottom figure.
C) Final model of subsurface structure. The offset of the fault is 200 m, as shown by the circle. Deeper structure with an offset of 1 km was needed to explain the long wave-length anomalies both of magnetic and gravity observation (upper and middle figures, respectively).

1.8 km, with 4 shot points in the Tajima and Hyogo rivers (**Fig. 12A**). The spacing of the sensors was between 25 to 30 m. An air gun of 5 cubic inches was used as the

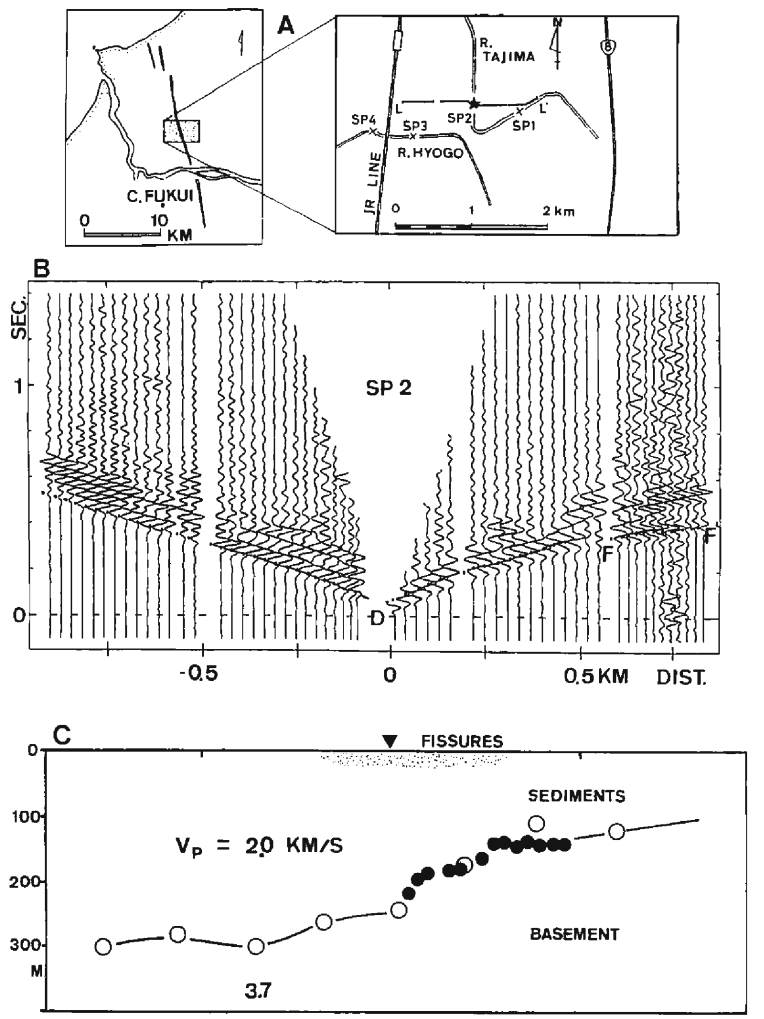

Fig. 12. Explanation for outline of the seismic exploration (modified after Amaike et al., 1984)[27].

A) Map showing the observation site. L–L′ in the right figure shows the observation line, which is almost identical with the main line.

B) An example of a record. The distance is measured from the source (SP2). Note that the first arrivals in the western region to the source show a constant velocity (1.6 km/s), while in the eastern region the same velocity can be traced as far as 0.5 km. At farther stations a faster velocity (2.0 km/s) is observed, suggesting that the basement is shallower in the eastern region than in the western region.

C) Proposed model of subsurface structure. Travel times from two natural earthquakes were also used for analysis.

source, and signals from 30 to 180 times of shots were stacked at each shot point. The sensors were velocity type vertical seismometers with a natural frequency of 8 Hz.

The most striking result is shown in the arranged seismograms for the shot point 2 (**Fig. 12B**), beneath which the fault is expected. *D* denotes one peak for each trace just after the first arrival. In the left half of the figure, this phase shows a constant velocity of 1.6 km/s, while in the right half, *D* phase can be seen only at distances of 0 to 0.5 km, and at farther stations, a much faster velocity of 4.9 km/s was observed. On analyzing the travel times, it was concluded that this phase was the seismic wave refracted at the basement rocks and that the depth to the basement rocks was shallower in the eastern half than in the western section. The depth to the basement in the western half of the figure was estimated to be over 270 m, because no refracted waves were recorded as the first arrival even at the most westerly point (around 1 km from the source) in the line. The results from the other 3 shots also supported these results.

Fortunately, the travel time data for two natural earthquakes were also obtained by chance. One took place when the sensors were deployed to the east of the shot point 2, and the other occurred during the observation of microtremors (Hurukawa et al., 1984)[28]. These data also were analyzed and a subsurface fault model (**Fig. 12C**) was obtained with a vertical offset of about 200 m, just agreeing with that of the above model derived from the gravity and magnetic data (**Fig. 10C**).

The dipping angle of the fault derived above is much smaller than that deduced from the fault movement associated with the 1948 event. This is because the present structure represents an assembly of small steps, each of which reflects the steeply dipping fault movement associated with a large event of the repeated earthquakes.

3.4 2-dimensional surveys along the fault strike

The vertical offset on the fault was determined to be about 200 m. Before using this value to estimate the recurrence time for the large earthquakes associated with the fault, it is necessary to confirm that the subsurface structure across the fault strike, at anywhere along the fault, is similar to that of the main line; because if the offset is generated by the repeated earthquakes, almost the same offset must exist at each point along the fault. We shall test this possibility.

First, the Bouguer anomalies along 5 other lines were observed and compared with those along the main line. The distribution of observation points is shown in **Fig. 13A**, together with that of the main line. As shown in **Fig. 13B**, they also show high values in the eastern part of each line and low values in the western part, just like that along the main line. The location of the fissure zone (triangles in **Fig. 13B**) coincides with the position of high gradient in the Bouguer anomaly.

Second, the long wave-length anomalies in the magnetic total force were also observed along 2 other lines (Takeuchi et al., 1983)[29], which again show a similar pattern to that of the main line (**Fig. 14A**). The aeromagnetic survey data were also plotted in the figure, which again shows the same pattern as along the main line.

Thirdly, microtremors were observed (Hurukawa et al., 1983[30], Hurukawa et al.

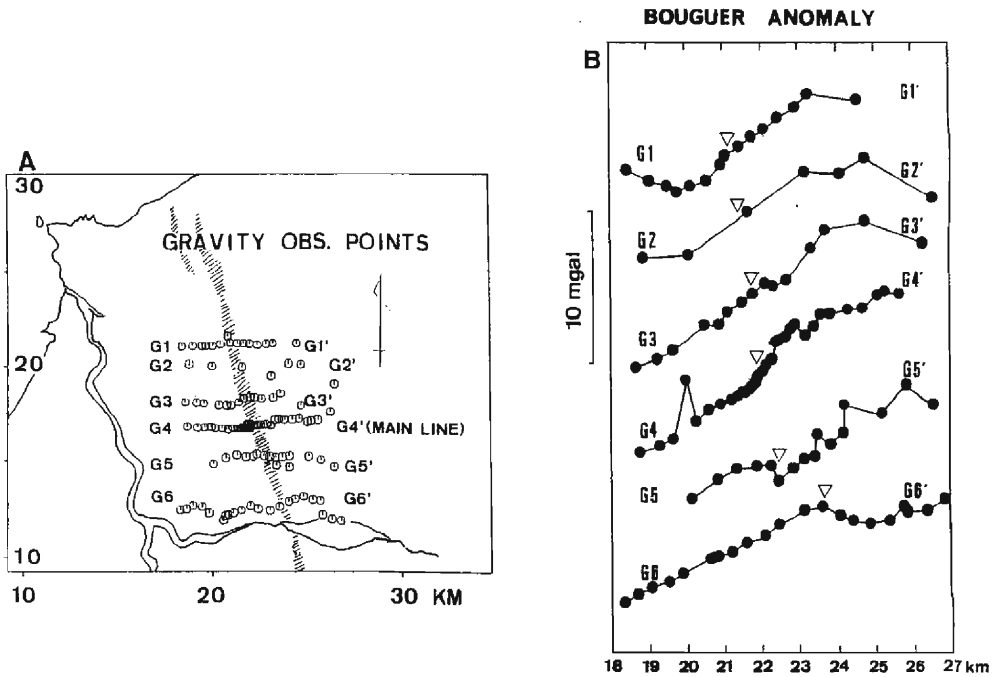

Fig. 13. **A**) Distribution of gravity observation points classified into six lines. G4–G4′ line is the main line.
B) Bouguer anomaly along the six lines. In each line, high values are distributed in the eastern region and low values in the western region. This indicates that the deeper structures beneath all the lines are similar to each other. Triangles show the location of the fault as suggested by the fissure distribution. The location of the highest gradient of the anomaly in each line is in close agreement with the location of the fault. This supports the fault having a comparable offset beneath these lines as beneath the main line.

1984[28]). Simultaneous observation at 8 points along the main line (Tajima line A1–A8 in **Fig. 15**) revealed that the microtremors with periods of 2 seconds abruptly changed their amplitudes across the Tajima river (**Fig. 16A**). Another simultaneous measurement was carried out along the same line but with a shorter spacing between the observation points (Tajima line C1–C8 in **Fig. 15**), in order to determine the fault location more accurately. The result was that the amplitudes changed between C-5 and C-6 (**Fig. 16B**). The predominant period of the microtremors was larger at the western points than at the eastern points. In **Fig. 16C**, an example of the waveforms of microtremors are presented. The difference is clear between points 1 to 5 and 6 to 8. The reason for the clear difference of amplitude is explained by the 'quarter wave-length law' (Tajime, 1957)[31]. The law predicts the predominant period of microtremors in the region west to the fault to be 1.33 to 2 sec (0.75 to 0.5 Hz) because the thickness of the sediments was 200 to 300 m and the average S-wave velocity was about 600 m/s[32]. Therefore, the amplitude of the microtremors with periods around 2 sec could be large in the region. In the eastern region to the fault,

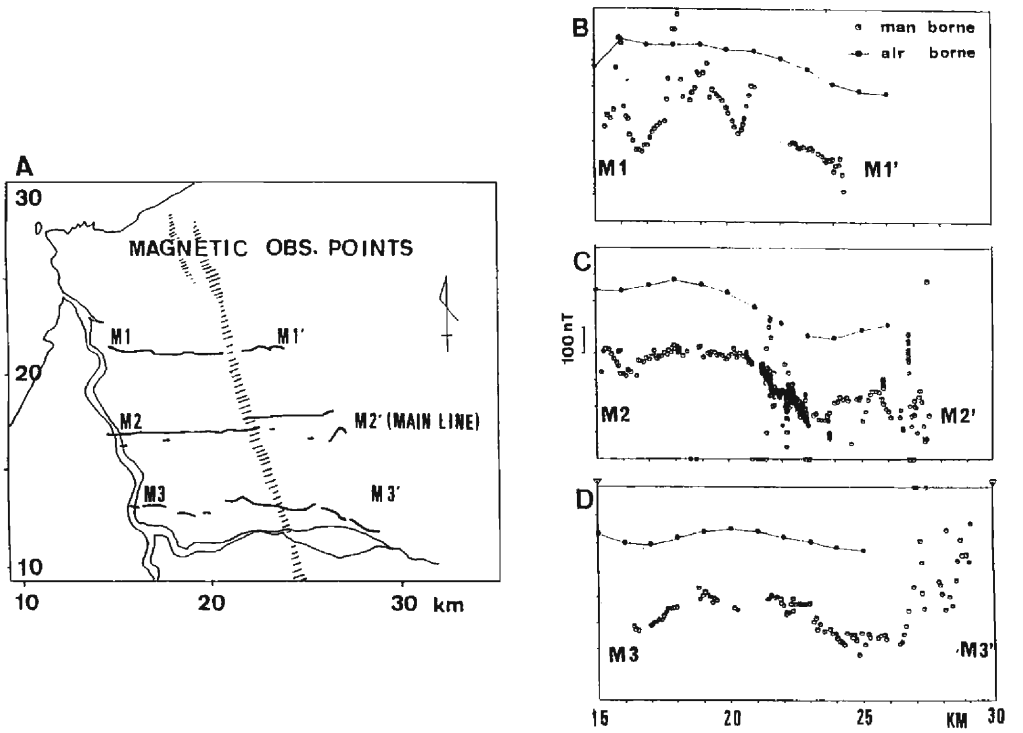

Fig. 14. **A**) Distribution of geomagnetic total force observation points along three lines. M2–M2′ is the main line.
B), **C**) and **D**) Observed anomalies along M1–M1′, M2–M2′ and M3–M3′ lines, respectively. Time variation was corrected. Air borne data are after Geological Survey of Japan.

the predominant period might be about 0.6 sec (1.6 Hz), and the microtremors with periods of about 2 sec might be smaller.

Takeuchi et al. (1984)[33] carried out a further measurement of microtremors along 4 lines (**Fig. 15**). In this case, a mobile observation system was employed, and time variations among microtremors were monitored at a fixed station in each of the lines. Along lines Shimozeki and Nagasaki, the microtremor amplitudes are greater in the western points than in the eastern points, as shown in the waveform examples (**Fig. 17A**), similar to the observation along the main line. But along lines Nagaya and Sadamune, such a tendency is obscure. To eliminate time variation of amplitude, the ratios of the amplitude at a mobile point to the fixed point were calculated (**Fig. 17B**). The results also showed a clear contrast across the fault along lines Shimozeki and Nagasaki, whereas along lines Nagaya and Sadamune, such a tendency was again obscure. This suggests that the offset of the basement rocks might be smaller here.

Finally, the difference of the ground surface levels across the fault (**Fig. 18**) was studied. No difference was recognizable to the naked eye in the actual field, because

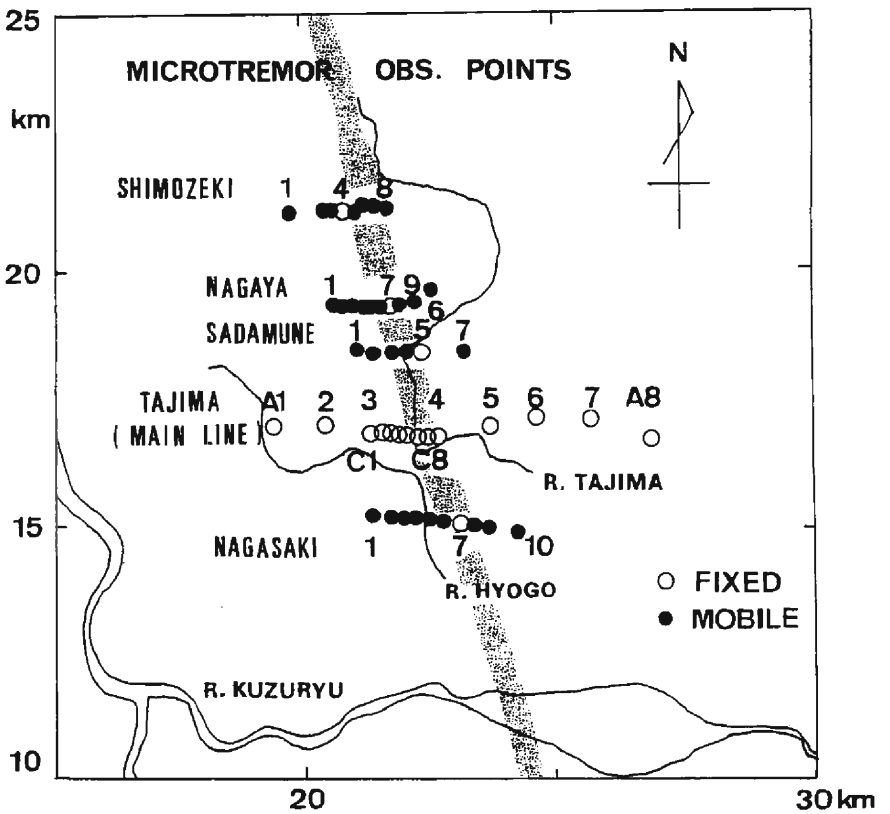

Fig. 15. Distribution of observation points for microtremors. Observation points are divided into five lines. C1–C8 are for a denser observation in Tajima A1–A8 line. C2 and C7 are identical with A3 and A4, respectively. Open circles denote fixed stations and solid ones are mobile stations. The shaded band is the fault trace as suggested by the fissure distribution.

topographic variations were very small and gentle over a long distance. But it can be visualized when plotted in a vertically exaggerated scale. The data of altitude are taken from large-scale topographic maps. Along the main line ($y=17$ km), a difference of 3 m can be detected between two points 1 km apart from each other across the fault. Other lines also show comparable amounts of differences, the maximum one being as large as 6 m. Common to all lines, the altitude increases to the east. Moreover, the locations of the slopes align themselves in a line which coincides with the fault strike (hatched) as shown in the figure.

All these evidences support existence of the fault anywhere beneath the fissure belt formed by the 1948 earthquake, and thus it is strongly suggested that the offset was generated by the repeated earthquakes.

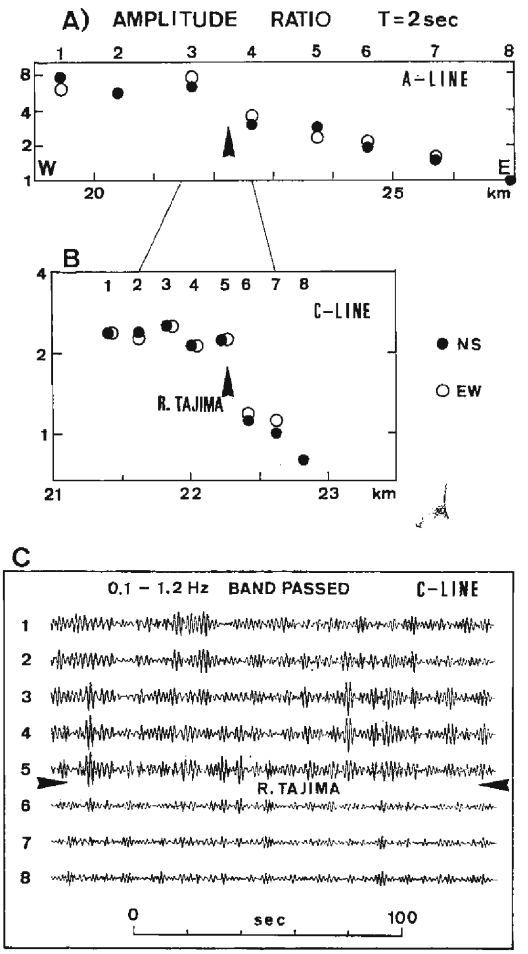

Fig. 16. Results from microtremor observation (modified after Hurukawa et al., 1984)[28].

A) Amplitude ratios of microtremors with a period of 2 sec. A8 is used as the standard. Arrow shows the location of R. Tajima which is in the fissure zone. The amplitude ratio change abruptly across R. Tajima.

B) Same ratios as figure A) along the line C1–C8, in which observation points were densely distributed between A3 and A4. Again abrupt change was found across R. Tajima.

C) Example of microtremor waveforms for C line. The abrupt change of the amplitude is very clear also in the waveform. Note that these traces were obtained simultaneously with one recorder, so that no temporal variation is included.

4. Average Recurrence Time of the Fukui Earthquake

The number of the earthquakes that have repeatedly occurred on this fault can be obtained simply by dividing the offset by the vertical displacement associated with

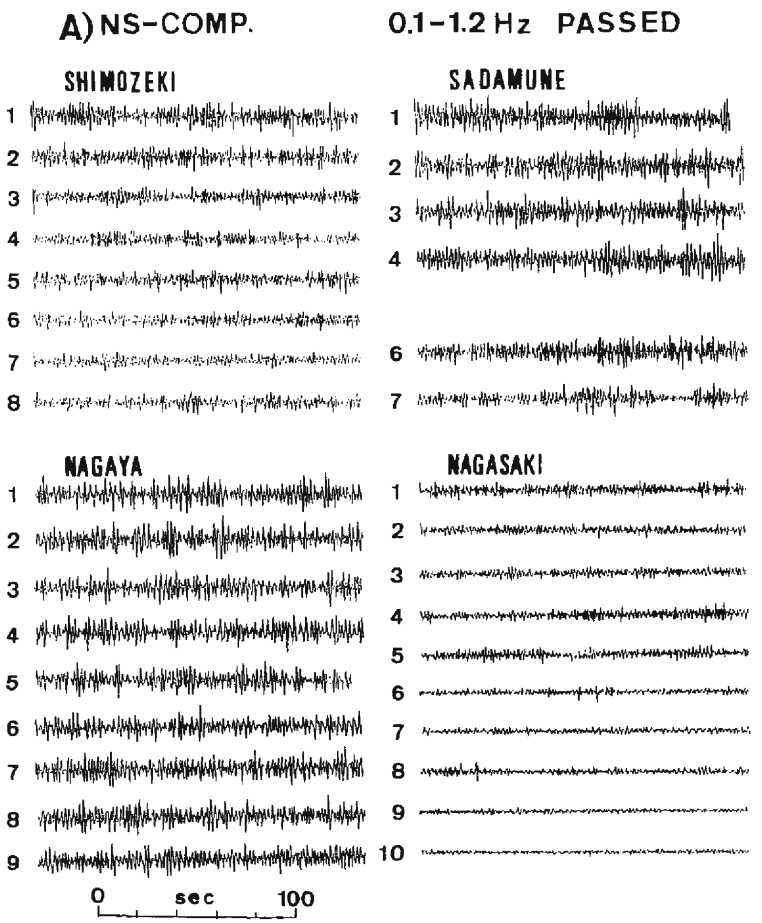

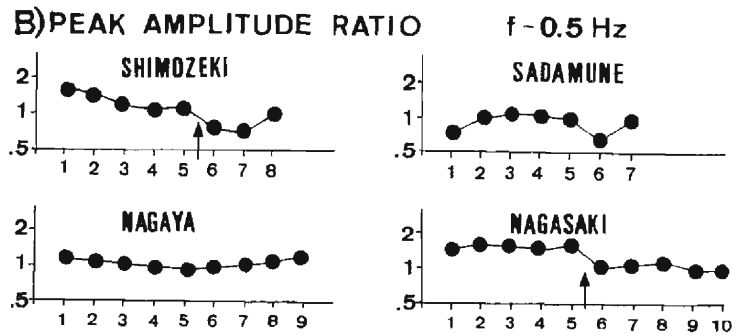

Fig. 17. **A**) Examples of microtremor waveforms in other lines than the main line. Waveforms do not show a clear difference in each line. As they were observed by employing mobile stations, time variations might conceal the local variations.

B) Amplitude ratios. Stations denoted by open circles in **Fig. 15** were

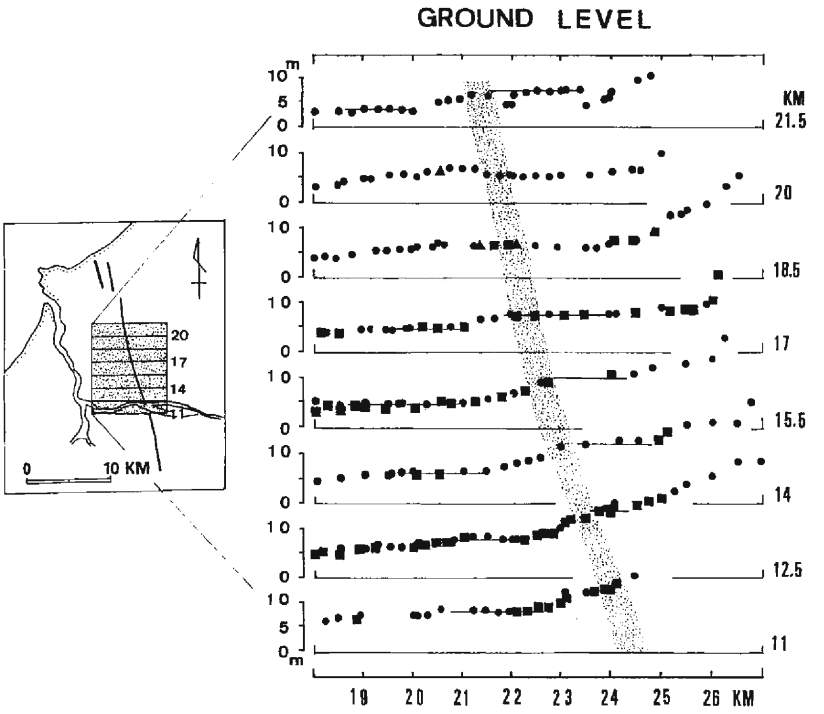

Fig. 18. Ground levels read from topographic maps plotted along eight lines (modified after Takeuchi and Amaike., 1985)[20]. Difference of level is shown in each line. Location of the difference coincides with the fault strike as shown by shaded band. However, the difference is obscure in lines of 18.5 km and 20.0 km. At both sides of the differences, flat regions are recognized.

one earthquake. The number would be 200, because the offset was determined to be about 200 m, and the vertical displacement associated with the 1948 event was around 1 m. The recurrence time is given by the total time length of the sequence divided by the number of earthquakes. The beginning time of the sequence was estimated as follows. Sugimura (1967)[34] found that the late Quaternary crustal movements in Japan have taken place with an almost uniform rate, and he estimated the beginning of the movements to be 1 to 2 million years ago. Matsuda (1976)[35] also considered that the major Quaternary faults in Japan began to move about one million years ago, and the sense of the movement has been the same since then. Ando (1979)[36] also supports their ideas, however he also states that the beginning time of the fault movement differs according to its location in Japan. In any case, the rate

used as standard points in each line. Time variations were corrected by plotting the ratio of amplitude at a mobile station to that of the simultaneously observed data recorded at the fixed point. In lines Shimozeki and Nagasaki, clear change of amplitude ratio can be seen across the fault. However, in lines Nagaya and Sadamune no such changes can be seen.

of movements in the last 500,000 years are almost constant all over the Japan islands. On the other hand, in the Fukui earthquake region, the basement structure was formed in the middle Quaternary (Hokuriku Nouseikyoku Keikakubu, 1982)[18], and the basement which consists of Tertiary rocks have been as a whole subsiding since middle Quaternary (Kaseno et al. 1972)[16]. Then the offset in the basement rocks may have been zero before they began to subside, and thus the vertical offset presently existing must be the accumulation of the vertical dislocations associated with the repeated earthquakes occurring since then. It is reasonable to assign 500,000 years ago to the time for the first event in the earthquake series, the vertical dislocations of which contributed to the vertical offset of 200 m. Then the average recurrence time can be estimated as 500,000 years / 200=2,500 years. The historical earthquake catalogue for Japan, which records events of the last 1,000 years or so, does not report any other earthquakes than the 1948 event generated by the fault. This is quite expected, if the recurrence time, as calculated above, be 2,500 years. However, this is an average estimation for the recurrence time, and it does not mean a perfectly cyclic occurrence of earthquakes.

5. Difference of the Ground Surface Levels

The average recurrence time was derived to be 2,500 years in the previous section. Then the topographic offset of the present ground surface could be produced by only one earthquake, i.e., the 1948 event. Here a new question arises as why the present surface level differences across the fault can exceed several times larger than the dislocation associated with the 1948 earthquake. The local variation of offset must also be explained. Similarly, the vertical offset in the boundary between the alluvial and diluvial deposits near the main line, 14 m from boring data (Hokuriku Nouseikyoku Keikakubu, 1977)[25] is too large for the boundary age of 11,000 years, since the expected total dislocations by the subsequent earthquakes is only 5 m as calculated from the average recurrence time of 2,500 years.

Here we propose an idea by which the amount of the actual offsets can be explained, together with the average recurrence time of 2,500 years. The idea is that the offset now existing in a certain layer is the sum of 1) the offset which had already been existing when the layer was formed, and 2) the offset that has been added afterwards. The latter alone should be used for estimation of the recurrence time. In our case, out of the vertical offset of 14 m, only an offset of 5 m may be due to 5 earthquakes including the 1948 event, in the last 11,000 years, using the average recurrence time of 2,500 years. The rest of the 9 m should have already existed there 11,000 years ago. Along the main line the surface level difference is about 3 m, which may be also divided into two parts, 2 m for a pre-existing difference and 1 m for the seismic dislocation by the 1948 event.

Another question may arise as to why the surface level varies from place to place. First, the effect of sedimentation which diminishes the surface offset should be taken into account. We have derived a tool for the quantitative treatment of this subject.

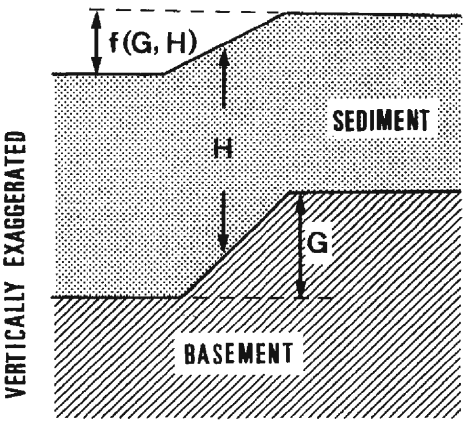

$$f(G, H) = G \times \exp(-b \times H)$$

Fig. 19. Schematic diagram showing the covering effect of sediments. For derivation of function $f(G, H)$, see appendix.

As illustrated in **Fig. 19**, we introduce a ramp-shape structure with an offset G, on which a sedimentary layer with a thickness of H has been deposited. The offset f in the surface of the sediment should be estimated. For simplicity let us take f to be a function of only G and H. Then $f(G, H)$ can be easily derived, as elaborated in the appendix, as,

$$f(G, H) = G * \exp(-b * H),$$

where b is a positive constant. Note that the offset G, which was the surface offset before sedimentation, is unchanged; however, it is no longer a surface offset but an offset in the underlying boundary.

Another factor that changes the offset is the earthquake occurrence. Its effect, however, is simple. The offsets both at the ground surface and in depth are equally increased by D, at each time of an earthquake occurrence.

5.1 Estimation for b value in f(G * H)

The value b in function f can be determined for the main line. Let us consider the change of the surface offset during the last 11,000 years. 11,000 years ago when the sedimentation of alluvial deposits possibly started, the surface of the diluvial sediments had an offset G_0. From the average recurrence time of 2,500 years, five earthquakes including the 1948 event are considered to have occurred in the last 11,000 years. From 11,000 years ago till just before the first one of the five earthquakes, sedimentation took place. So the offset G_1 at the surface just before the earthquake can be expressed as

$$G_1 = G_0 * \exp(-b * H_1),$$

where H_1 is the thickness of the overlying sediments. The sedimentation rate R is

estimated to be almost constant during the last 16,000 years from boring core data, whose ages were determined with a ^{14}C dating method (Nihon Tetsudou Kensetsu Koudan Nagoya Shisha and Kiso Jiban Konsarutantsu Kabushiki Kaisha, 1984)[37].

$R=3$ m/1,000 years.
$H_1=R * T_1$.

The first earthquake of the five increased the offsets both at the surface and the boundary between the alluvial and diluvial sediments by D, so the new offset G_1' is,

$$G_1'=G_1+D$$
$$=G_0 * \exp(-b * H_1)+D.$$

Sedimentation continued until the next earthquake, and the same process repeats until now. Thus, after n-th event, the surface offset G_n' can be expressed as,

$$G_n'=G_n+D$$
$$=G_{n-1}' * \exp(-b * H_n)+D \quad (n=1, 2, \ldots, 5), \text{ where}$$
$H_n=R * T_n$ and
$G_0'=G_0$.

On the other hand, the present offset between the alluvial and diluvial sediments can be simply estimated as

$$G_0+n * D.$$

The observed data along the main line are as follows.

$G_5'=3$,
$G_0+n * D=14$. The other parameters were assumed as,
$n=5$,
$T_n=2{,}500$ $(n=2, 3, 4, 5)$,
$T_1=1{,}000$
$D=1$.

Substituting these values into the above formula, we obtain the value for b. **Figure 20** illustrates our estimation. The horizontal axis gives the age of the layers and the vertical one shows the offset. Curves are plotted for different values of b. Clearly the present offset of the ground level is much affected by b, and $b=0.07$ can best explain the actual offset (difference) of 3 m along the main line. The earthquakes were assumed to occur with a constant interval of 2,500 years in the derivation. However, the same estimation for b was obtained even when the intervals were changed within a certain limit, as long as the total number of earthquakes remained five. The value $b=0.07$ will also be used to explain the offsets in other lines.

5.2 Simulation of the Ground Level difference

The purpose of this section is to simulate the difference in the present ground level, using the data of the offset at the alluvial-diluvial boundary together with the function $f(G, H)$. Substituting $b=0.07$, as derived above, into the function, we will

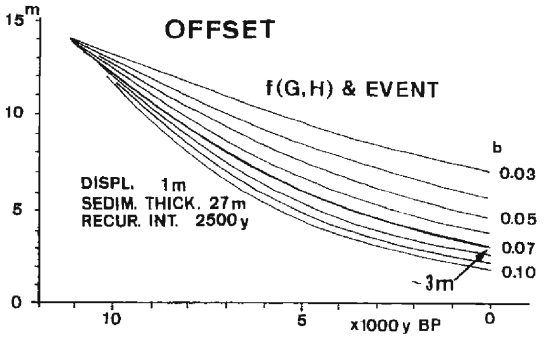

Fig. 20. Examples of the calculated offsets in the subsurface layeres for the main line. Horizontal axis represents age of layers. The offset in the boundary between alluvial and diluvial deposits was assumed to be 14 m. Function $f(G, H)$ was used for estimating the effect of sedimentation, and earthquake occurrence with a recurrence time of 2,500 years was assumed. Other parameters are shown in the figure. Curves are drawn for different b values. b=0.07 was best to explain the surface offset of 3 m, which presently exists along the main line.

estimate sedimentation effect. The vertical displacements for the earthquakes were taken from Hasegawa's model (1986)[5], and 2,500 years was again used for the average recurrence time. The rate of sedimentation is calculated from the thickness of the alluvial sediments and the topographic maps. The thickness of the sediments is estimated from a contour map deduced from the data of more than 100 well borings performed in the area concerned (Hokuriku Nouseikyoku Keikakubu, 1977)[25]. The vertical offsets of the boundary between alluvial and diluvial deposits are also read from the depth contours. The calculated results for 8 lines are shown in **Fig. 21A**, where the distances are measured in the N-S direction, and the data used are shown in **Fig. 21B** and **21C**. The actual differences are shown by solid circles, which are read from **Fig. 18**. They are defined as the differences of the levels at two points located respectively at 2 km westward and 1 km eastward from the fault trace. The reason for this selection is that the ground surface near these two points is flat, and hence the difference could be uniquely defined. Six out of the eight calculated values can satisfactorily simulate the actual differences. Thus, the local variation of the differences of the ground surface levels is explained as the result from the repeated earthquakes and also from sedimentation. Moreover, shorter recurrence times were not needed to explain the large differences that exceed the vertical dislocation associated with the 1948 event. Thus, the long term slip rate of the fault in Holocene is possibly the same as one averaged over the last 500,000 years.

The calculated values for the lines y=18.5 km and 20.0 km are significantly larger than the observed ones, where the actual differences are almost zero. This means that either b=0.07 is not a good value, or the vertical dislocations associated with the earthquakes in the last 11,000 years were very small (or almost zero) for the two lines. The former possibility is difficult to ascertain. Larger values for b give better fitting

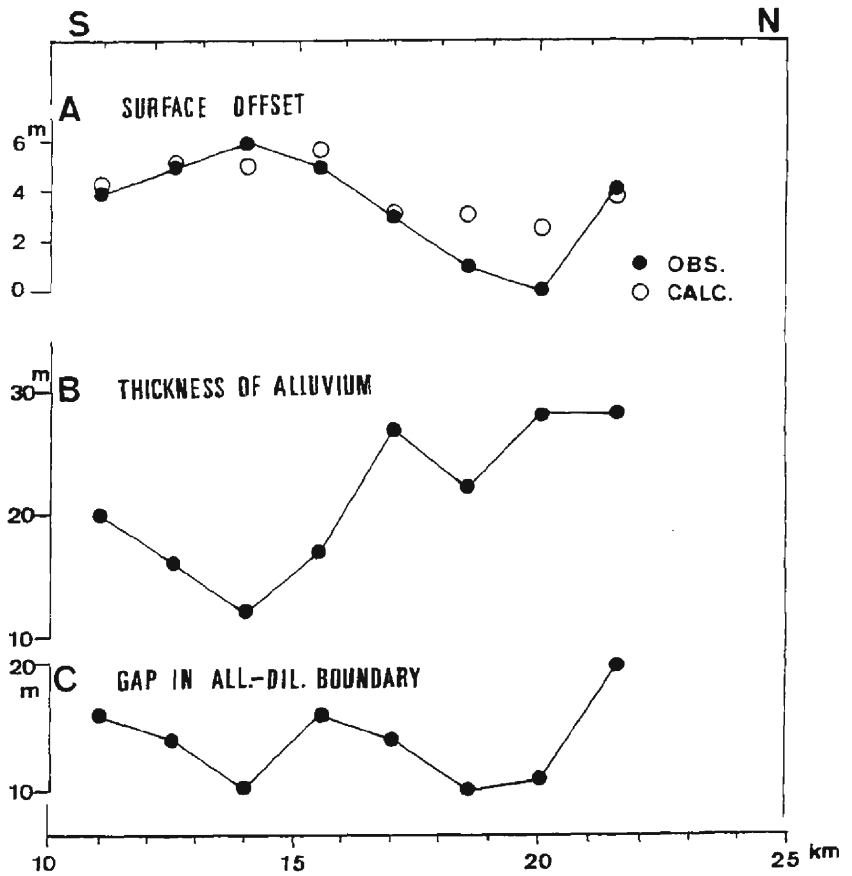

Fig. 21. **A)** Calculated surface offsets (open circles) and observed ones (solid circles). Six calculated values agree well with the observation. Observed values at lines $y=18.5$ and 20.0 km are significantly smaller than calculated. For calculation, the offset at the boundary between alluvial and diluvial sediments (bottom figure) and thickness of the alluvial deposit (middle figure) were used.
B) Thickness of the alluvial deposit.
C) Offset in the boundary between alluvial and diluvial sediments.

for the two lines, but worse for the other 6 lines. Different values of b for each of the lines give a better result. However, that would be too speculative at present, because f represents only a simplified estimation and because the detailed sedimentation process is presently unknown.

The latter possibility that the vertical dislocations were very small for the two lines, however, can be justified in the next section where we discuss an aseismic region in the aftershock area of the 1948 event.

6. Present Aseismic Region in Relation to the Repeated Earthquakes

Microearthquake hypocenters in the aftershock area of the 1948 Fukui earthquake were relocated using P onsets observed by the Hokuriku Microearthquake Observatory (HMO), Kyoto University. The location program is based on the 'Hypocenter' by Lienert et al. (1986)[38]. It uses only P arrival times and determines the hypocenters by a damped least square method. Our observation network consists of 7 stations. The area concerned in this study is in the midst of the network; hence the hypocenters can be redetermined with more than 4 P onsets. The detectability is below $M=1$. The subsurface structure was assumed to have a constant P wave velocity of 5.9 km/s. This value was selected out of several velocities varying from 4.5 to 6.5 km/s because the number of events accurately determined was largest for this value.

The epicenters thus determined are plotted in **Fig. 22** for the period from May 1976 to Dec. 1984, that is from 28 to 36 years after the 1948 main shock. It shows a belt-like distribution along the Fukui earthquake fault. A clear aseismic region, ellipsoidal in shape, appears adjacent to the middle part of the fault. The major and minor diameters of the ellipse are 10 and 4 km, respectively.

The same aseismic region can also be seen in a seismicity map using JMA (Japan Meteorological Agency) data for about 1 month after the 1948 event (**Fig. 23**). The shape and dimension match well with those derived from the data of HMO, but the location, as revealed by the JMA data file, is biased several km west of that deduced

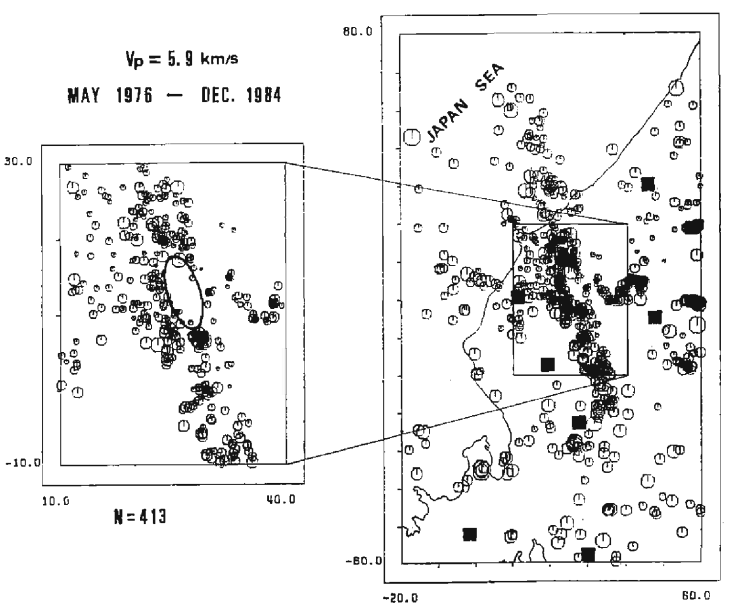

Fig. 22. Relocated epicenters in and around the aftershock area of the Fukui earthquake for the period from May 1976 to Dec. 1984. A clear aseismic region, ellipsoidal in shape, is shown. Solid squares in the right figure denote the stations used for hypocenter determination.

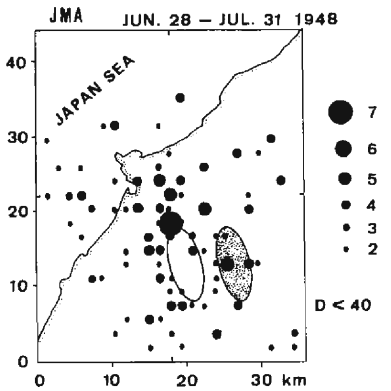

Fig. 23. Distribution of aftershocks for about 1 month just after the 1948 event. Plotted are the JMA data using SEIS-PC program[1]. The aseismic region as shown by open ellipse is located several km west to that found in **Fig. 22**. However, these two locations are concluded to be the same. See text for more detail.

from the HMO data file. However, the main shock is also located by JMA data several km west of the HMO aseismic region. The main shock undoubtedly originated from the fault, and the fault has been accurately located by our surveys near the western edge of the HMO aseismic region. We may thus conclude that these two aseismic regions are the same and the observed difference in location is just an artifact of the low accuracy of JMA data of over 40 years ago.

It is now clear that the aseismic region was created just after the main shock and has continued to exist until now. This aseismic region may have sustained enough stress before the 1948 earthquake, and was totally destroyed due to the release of much of the energy coseismically. As a result, the displacement associated with the earthquake was large. In fact, almost all the houses in and around this region totally collapsed (Tsuya, 1950)[2], and the displacement calculated by Hasegawa (1986)[5] is also large around here.

The location of the aseismic region is compared with that of the topographical offsets in the ground surface studied in the previous section. In **Fig. 18**, the ground level shows two flat areas, one being located to the west and the other to the east of the fault trace, and between these two areas the ground surface gently dips towards the west. White and black stripes in **Fig. 24A** denote the flat and the sloping regions, respectively. The east edges of the black stripes make a straight line, which coincides with the fault trace denoted by E1. And taking into account the dipping angle of the fault as illustrated in the cross section (**Fig. 24B**), the fault seems to limit the western edge of the aseismic region.

The agreement between the areas of the large differences of the ground level and the aseismic region is reasonable, since the aseismic region seems to have released much of its stress and consequently has lost the ability to generate aftershocks.

Just north to the aseismic region, the ground level differences across the fault

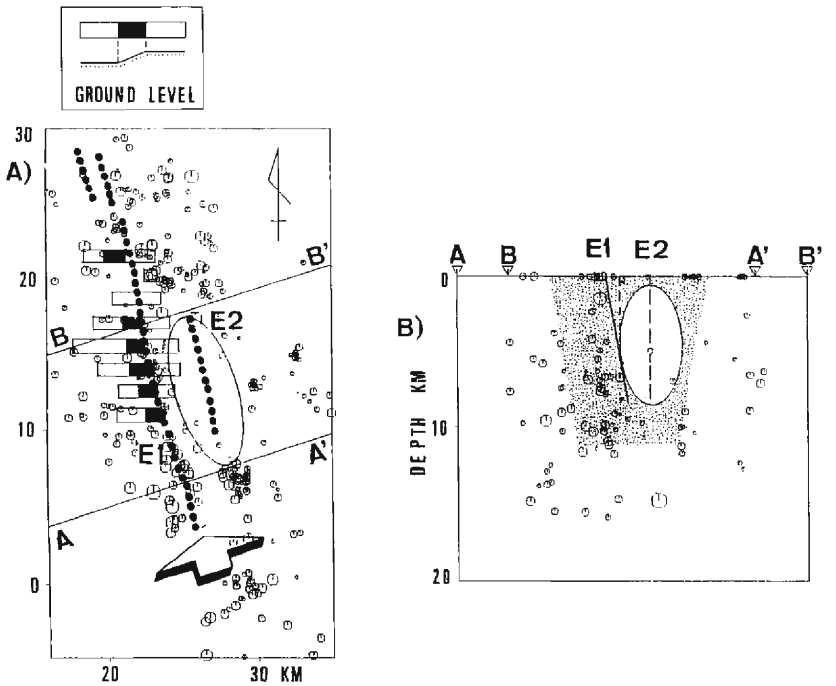

Fig. 24. **A**) Map showing the locations of two faults (E1 and E2) and the aseismic region. White and black stripes indicate the regions where the ground surface is flat and sloping, respectively, as indicated schematically in the top figure. The eastern end of the black stripes coincides with the fault trace (E1). The fault plane is also coincident with the western edge of the aseismic region, as shown by a cross section in the right figure.
B) Vertical cross section of hypocenters to demonstrate that the fault plane E1 limits the western edge of the aseismic region. For the dip angle of the fault E1, 80° was used as suggested by Hasegawa's model[5]. The fault plane of E2 is drawn as vertical, however, the actual dip angle is presently unknown.

(y=18.5 km and y=20.0 km) were very small as shown in the previous section. This is also reasonable, because the region may not have released much stress at the time of the 1948 Fukui earthquake and the resulting ground deformation was small.

Furthermore, we have to remember that the present topography reflects not only the dislocation of the 1948 earthquake but also those accumulated by the previous events. If the dislocations associated with the previous events were significantly small near the present aseismic region, the ground level differences of 3 to 6 m cannot be expected. Similarly, it is hardly the case that the previous dislocation was remarkably large in the region where the present ground surface is almost flat. In short, the previous events of at least the last 11,000 years took place with more on less the same distribution pattern of vertical dislocation as that of the 1948 event.

7. Discussion and Additional Remarks

The vertical offset on the Fukui earthquake fault was determined to be about 200 m. The beginning time of the earthquake sequence that has contributed to the offset was estimated to be 500,000 years ago. Then the long term rate of fault movement can be calculated as 200 * 2/500,000=0.8 (m/1,000y), where the multiplier of 2 was used to convert vertical dislocation to total one, referring to the case of the 1948 event.

No creep movement has been found for the faults in Japan (e.g. Abe et al., 1985)[39]. Moreover, in the central part of Japan (including the Fukui earthquake region), the average rate of seismic moment release due to earthquakes in the last 400 years is almost the same as that determined from geological slip on Quaternary faults during the late Quaternary (Wesnousky et al., 1982)[40]. These facts support the above calculated rate of the fault movement being almost identical with the long term slip rate of faulting. The Fukui earthquake fault is thus of B class activity after Matsuda's classification (1975)[6]. Matsuda[6] also deduced an empirical formula for the recurrence time from large recent earthquakes excluding the Fukui earthquake. Substituting the long term slip rate of 0.8 (m/1,000 y) into the formula, we obtain an average recurrence time of 2,275 years for $M=7.1$ earthquakes. Our estimation of 2,500 years agrees very well with the empirical estimation, and thus justifying the formula.

Besides the main portion of the Fukui earthquake fault described above, there is another short earthquake fault associated with the 1948 event (The Research Group for Active Faults, 1980)[41]. There is a possibility that the short fault also ruptured at the time of the 1948 Fukui earthquake, because the leveling surveys which were carried out after the earthquake revealed a small amount of vertical dislocation (Tsuya, 1950)[2] across that fault.

As cited in the introduction, the event of the 1948 Fukui earthquake consisted of at least two large earthquakes, the former being smaller and followed by the later one after 9 sec. Kanamori (1973)[4] successfully composed a theoretical waveform of these two large events by assuming that both of the events originated from the main fault but with different dislocations; the later one with four times larger dislocation than the earlier one. However, he attributed both events commonly to the main fault, only because of simplicity and possibly because the time accuracy of the available records was not enough to distinguish the hypocenter of the second event from that of the first one. In **Fig. 24A**, the locations of the two faults together with the aseismic region are represented. The shorter fault (E2) comes to the middle part of the aseismic region and the fault length coincides with its major diameter. It seems to be possible that the former (smaller) event originated from the shorter fault. In order to satisfy the condition that the amplitude of the waveform for the former event is 1/4 as large as that of the later event, the dislocation of the shorter fault needs to be 3/4 that of the main fault, since the length of the shorter fault is about 1/3 as long as that of the main fault and the width of the two faults are possibly the same. The leveling

survey across the shorter fault revealed a westward upheaval, although the initial motions of the waveforms of the first and the second shocks obtained at Abuyama show the same polarity. However, this can be explained as follows. An eastward upheaval with a little smaller dislocation than that of the later one was associated with the first (smaller) earthquake on the shorter fault. Then, after 9 sec, the later (larger) eastward upheaval associated with the main fault followed, when the coupling between the both side surfaces of the shorter fault might be weak. The western side surface of the shorter fault could upheave almost freely; the eastern side surface might not upheave as much as could be expected if the coupling was strong. Thus, the total deformation across the shorter fault could result in a westward upheaval. Moreover, the existence of the shorter fault may be the cause for the aseismic region to be located east to the main fault while the opposite side region is seismically active.

At the lower boundary of the basement rocks just beneath the present fault, a ramp-shape structure was also determined dipping to the west with an offset of 1 km. One may try to divide the offset of 1 km by the same rate of the long term vertical slip for the Fukui earthquake fault in order to calculate the starting time. However, it might be misleading to assume a constant slip rate back to Tertiary. It is better only to assume that the ramp-shape structure had existed before the Quaternary, regardless of whether it had been formed by earthquakes or not. However, in any case, this structure might have generated a weak lineation in the crust throughout the Quaternary, and this lineation might be responsible for the earthquakes of the last 500,000 years.

8. Conclusions

Recurrence characteristics of the large earthquakes associated with the Fukui earthquake fault were revealed and some additional points were also obtained. The main conclusions are as follows.

1) The existence of a fault associated with the 1948 Fukui earthquake was revealed by geophysical explorations such as gravimetric and magnetic surveys. The location coincides with the fissure zone that was formed by the 1948 event.

2) The vertical offset of the fault in the boundary between the basement rocks and the overlying sediment was estimated to be about 200 m beneath the main line. The ground surface topography and other exploratory surveys revealed that the fault can be traced not only along the main line but also along several lines almost parallel to it.

3) The vertical offset in the basement has been accumulated by the 200 previous earthquakes. An average recurrence time of 2,500 years was obtained for the earthquakes, because the 200 earthquakes may have occurred in the last 500,000 years. The long term slip rate of this fault was determined to be about 0.8 m/1,000 y and the activity of the fault is classified as B according to Matsuda's notation[6].

4) An aseismic region of elliptic shape was revealed in the hypocenter distribution of recent micro-earthquakes in and around the aftershock area of the 1948

Fukui earthquake. The west edge of the region coincides with the present fault. The region is revealed to have been aseismic since just after the 1948 event, because a region of similar extent and location was recognized in an epicentral distribution map drawn for one month after the main shock using JMA data.

5) A simple calculation method was proposed for assessing the effect of alluvial sedimentation. By using this method, the local variation of the differences of the ground levels across the fault was explained. The fact is also well explained that the differences in some traverses exceed the vertical dislocation associated with the 1948 event. For the calculation, occurrence of five earthquakes in the last 11,000 years was assumed, as suggested by the average recurrence time derived. Since the differences of the surface topography are significantly small to the north of the aseismic region, the vertical dislocations of the repeated earthquakes, at least those occurring during the last 11,000 years, might be equally small.

6) In addition, in the central part of the aseismic region, another fault was located with a length almost equal to the major diameter of the region. The first smaller one in the multiple events of the 1948 main shock may possibly have been generated by the shorter fault. By assuming this, the westward upheaval across the shorter fault as revealed by the leveling surveys can be explained.

9. Acknowledgement

The author expresses his thanks to Y. Kishimoto and K. Oike for their valuable discussions and encouragement throughout the study and also for their critical reading of the manuscript. Thanks are also due to T. Mikumo, Y. Kobayashi, H. Watanabe, M. Ando, N. Hurukawa, R. Ghose and anonymous referees for critical reading of the manuscript. This work was partly based on the results of the geophysical explorations carried out in cooperation with N. Hirano, Y. Kono, M. Satomura, N. Hurukawa, F. Amaike, S. Kasuga, K. Nishigami, Y. Kawabe, T. Imazumi, S. Abe, N. Furuse, M. Sunami, T. Imai, H. Murakami and K. Anada. The author appreciates their kind cooperation. N. Sumitomo, K. Matsumura and K. Nakamura are also appreciated for their advice in observation and data analysis. People at Sakai and Maruoka towns, Fukui prefecture, were kind enough to allow us to use their rice fields and buildings as our test sites. Y. Kono, N. Hurukawa, F. Amaike, K. Watanabe, T. Shibutani and T. Ohkura encouraged the author throughout the study. The author also thanks them.

References

1) Ishikawa, Y., K, Matsumura, H. Yokoyama and H. Matsumoto: SEIS-PC —its outline—, Jyoho Chishitsu, 10, 1985, pp. 19–34 (in Japanese with English abstract).
2) Tsuya, H.(editor): The Fukui earthquake of June 28. Report of the special committee for the study of the Fukui earthquake, 1950, pp. 197.
3) Hirono, T.: Observed Results of the Fukui Earthquake recorded by Seismometers, Chousa Kenkyuu Sokuhou, Nihon Gakujyutsu Kaigi, 1949, pp. 15–25 (in Japanese).

4) Kanamori, H.: Mode of strain release associated with major earthquakes in Japan, Ann. Rev. Earth Planet. Sci., 1, 1973, pp. 213–239.
5) Hasegawa, Y.: Non-linear Inversion Technique for Geodetic Data Analysis, Master Thesis of Tokyo Univ., 1986, pp. 44 (in Japanese).
6) Matsuda, T.: Magnitude and recurrence interval of earthquakes from a fault, J. Seismol. Soc. Japan, Vol. 28, 1975, pp. 269–283 (in Japanese with English abstract).
7) Ando, M., T. Tsukuda and A. Okada: Trenches across the 1943 Trace of the Shikano Fault in Tottori, Rep. coordin. Commit. Earthq. Predic., Vol. 23, 1980, pp. 160–165 (in Japanese).
8) Okada, A., M. Ando and T. Tsukuda: Trenches across the Yamasaki Fault in Hyogo Prefecture, Rep. coordin. Commit. Earthq. Predic., Vol. 30, 1981, pp. 376–381 (in Japanese).
9) Disaster Prevention Research Institute, Kyoto University: Trenches across the Trace of the 1891 Nobi Earthquake Fault, Rep. coordin. Commit. Earthq. Predic., Vol. 29, pp. 360–367 (in Japanese).
10) Disaster Prevention Research Institute, Kyoto University: Trenching Excavation at the Atotsugawa Fault, Central Japan, Rep. coordin. Commit. Earthq. Predic., Vol. 30, 1983, pp. 376–381 (in Japanese).
11) Wallace, R. E.: Earthquake recurrence intervals on the San Andreas fault, Geol. Soc. Am. Bull., Vol. 81, 1970, pp. 2875–2890.
12) Fukui Prefecture: Explanations for the Geological Map of the Fukui Prefecture region, 1969, pp. 117 (in Japanese).
13) Hokuriku Nouseikyoku Keikakubu: Micro-topographical Province of the Sakai Plain, 1982, pp. 67 (in Japanese).
14) Geographical Survey Institute: Horizontal Strain in Japan 1985–1883, 1987, pp. 133.
15) Takeuchi, F.: Relocation of microearthquakes along the Fukui Earthquake Fault and their Focal Mechanisms, Prog. Abstr. Seismol. Soc., Japan 2: 1988, p. 128 (in Japanese).
16) Kaseno, Y., S. Miura and S. Fujii: Construction Process of the Coastal Plains in the Hokuriku District, Chishitugaku Ronshuu, Vol. 7, 1972, pp. 91–100 (in Japanese).
17) Takeuchi, F. and N. Hirano: On seismicity maps by the Hokuriku Microearthquake Observatory–Summary of data for about 10,000 events–, Ann. Disast. Prev. Res. Inst., Kyoto Univ., Vol. 28, B-1, 1985, pp. 157–170 (in Japanese with English abstract).
18) Suzuki, K.: Gravity Anomaly over the region of Fukui Prefecture, Graduation Thesis of Kanazawa Univ., 1982, pp. 37 (in Japanese with English abstract).
19) Takeuchi, F., N. Hirano, M. Satomura and Y. Kono: Observation of gravity to reveal a buried fault associated with the Fukui Earthquake, Bull. disast. Prev. Res. Inst., Kyoto Univ., Vol. 33, 1983, pp. 147–162.
20) Takeuchi, F. and F. Amaiki: Ground level gaps generated by the 1948 Fukui earthquake and its previous events, recognized on topographical maps, J. Seismol. Soc. Japan, Vol. 1985, pp. 141–143 (in Japanese).
21) Hibi, T.: Gravity Anomaly over the Northern Part of Central Japan, Graduation Thesis of Kanazawa Univ., 1982, pp. 40 (in Japanese with English abstract).
22) Geological Survey of Japan: Total Intensity Aeromagnetic Map off the Coast of Wajima-Fukui Area (2–2), 1975.
23) Talwani, M., J. L. Worzel and M. Landisman: Rapid Gravity Computation for Two-Dimensional Bodies with Application to the Mendocino Submarine Fracture Zone, Journal of Geophysical Research, 64 No. 1, 1959, pp. 49–59.
24) Grant, F. S. and G. F. West: Interpretation Theory in Applied Geophysics, McGraw-Hill Book Co., 1965, pp. 319–324.
25) Hokuriku Nouseikyoku Keikakubu: Hydrogeology and ground water in Fukui Prefecture, 1977, pp. 48 (in Japanese).
26) Kono, Y., M. Sunami and M. Fujii: Relationship between gravity anomaly and earthquake hazard in the Fukui Plain, Central Japan, J. Seismol. Soc. Japan, Vol. 34, 1981, pp. 377–383 (in Japanese with English abstract).
27) Amaike, F., F. Takeuchi, S. Kasuga, N. Hurukawa and N. Hirano: Seismic exploration of the

buried fault associated with the Fukui Earthquake, 1948 and its tectonic implications, J. Seismol. Soc. Japan, Vol. 37, 1984, pp. 441–452 (in Japanese with English abstract).
28) Hurukawa, N., S. Kasuga, F. Takeuchi and F. Amaike: Investigation of the Fukui-Earthquake Fault by means of array observation of microtremors, J. Seismol. Soc. Japan, Vol. 37, 1984, pp. 205–215 (in Japanese with English abstract).
29) Takeuchi, F., N. Hirano and N. Hurukawa: Geophysical Exploration for the Fukui Earthquake Fault—Part 1, Geomagnetic Total Force Method, Prog. Abstr. Seismol. Soc. Japan, No. 1, 1983, p. 219 (in Japanese).
30) Hurukawa, N., F. Takeuchi, S. Kasuga, N. Hirano and F. Amaike: Observational Study on 1- to 5-sec microtremors around the Fukui Earthquake fault in the Fukui Plain. Annuals. Disast. Prev. Res. Inst., Kyoto Univ., 26b, 1983, pp. 123–134 (in Japanese with English abstract).
31) Tajime, K.: Minimum Group Velocity, Maximum Amplitude and Quarter Wavelength Law. Love-waves in Doubly Stratified Layers, J. Phys. Earth, Vol. 5, 1957, pp. 43–50.
32) Amaike, F.: Seismic explorations of the buried fault associated with the 1948 Fukui earthquake, J. Phys. Earth, Vol. 35, 1987, pp. 285–308.
33) Takeuchi, F., N. Hurukawa and N. Hirano: A Trial to determine the Strike of the Fukui Earthquake Fault by Micro-tremor Observation, Prog. Abstr. Seismol. Soc. Japan, No. 1, 1984, p. 225 (in Japanese).
34) Sugimura, A.: Uniform Rates and Duration Period of Quarternary Earth Movements in Japan, J. Geoscience, Osaka City Univ., Vol. 10, 1967, pp. 25–35.
35) Matsuda, T.: Empirical Rules on Sense and Rate of Recent Crustal Movements, J. Geodetic Society of Japan, Vol. 22, 1976, pp. 252–263.
36) Ando, M.: Tctonic Stress Field of the Japan Islands for the last 0.5 million years, Gekkan Chikyuu, Vol. 1, 1979, pp. 541–546 (in Japanese).
37) Nihon Tetsudo Kensetsu Koudan Nagoya Shisha and Kiso Jiban Consultants Co.: Geological Report for the Hokkan Fukui Tsuruga Regions 21, 1984, pp. 35 (in Japanese).
38) Lienert, B. R., E. Berg and L. N. Frazer: HYPOCENTER: An Earthquake Location Method Using Centered, Scaled, and Adaptively Damped Least Squares, Bull. Seismol. Soc. Amer., Vol. 76, No. 3, 1986, pp. 771–784.
39) Abe, K., A. Okada and T. Kakimi (editors): Earthquakes and Active Faults, ISU Co, 1985, p. 695 (in Japanese).
40) Wesnousky, S. G., C. H. Scholz and K. Shimazaki: Deformation of an Island Arc: Rates of Moment Release and Crustal Shortening in Intraplate Japan Determined from Seismicity and Quaternary Fault, J. Geophys. Res., Vol. 87, No. B8, 1982, pp. 6829–6852.
41) The Research Group for Active Faults: Active Faults in Japan, University of Tokyo Press, 1980, pp. 363 (in Japanese).

Appendix

Derivation of function $f(G, H)$

We may assume some reasonable characteristics for f. If there are no sediments, nothing occurs to the offsets.

1. $f(G, 0)=G$, for any G.
   Too thick sediment conceals the offset entirely.
2. f tends to 0 if H tends to infinity.
   Sedimentation effect is additive.
3. $f(f(G, H_1), H_2)=f(G, H_1+H_2)$.
   We assume that f can be separated by parts as,
4. $f(G, H)=g(G) * h(H)$. From 1. and 4.,
   $f(G, 0)=g(G) * h(0)=G$. Then,

$g(G)=G/h(0)$, where $h(0)$ is a constant. So,

$f(G, H)=G * h(H)/h(0)$. Substituting this into 3 we get,

$f(G*h(H_1)/h(0), H_2)=G * h(H_1+H_2)/h(0)$. Again using the above expression,

$G * h(H_1)/h(0) * h(H_2)/h(0)=G * h(H_1+H_2)/h(0)$. Therefore,

$h(H_1) * h(H_2)/h(0)=h(H_1+H_2)$. Differentiating both sides by H_1 yields,

$h'(H_1) * h(H_2)/h(0)=h'(H_1+H_2)$, where $'$ denotes d/dH_1.

Similarly, differentiating by H_2 leads to,

$h(H_1) * h'(H_2)/h(0)=h'(H_1+H_2)$. Equating these two,

$h'(H_1)/h(H_1)=h'(H_2)/h(H_2)$. The left hand side is a function of H_1 alone and the right of H_2. These two can be equated only when they are constant. Let the constant be $-b$, where b is positive so as to satisfy condition 3.

$-b=h'(H_1)/h(H_1)=d(\ln h(H_1))/dH_1$. Then,

$h(H)=C * \exp(-b * H)$, where C is a constant and H_1 is replaced by H.

Thus, $f(G, H)$ is now expressed by,

$f(G, H)=C/h(0) * G * \exp(-b * H)$. With condition 1,

$f(G, 0)=G=C/h(0) * G * 1$, then $C/h(0)=1$. Finally,

$f(G, H)=G * \exp(-b * H)$. (qed.)